Please cite this article in press as: Kozawa et al., The CD44/COL17A1 pathway promotes the formation of multilayered, transformed epithelia, Current Biology (2021), https://doi.org/10.1016/j.cub.2021.04.078

Current Biology

CellPress

Article

The CD44/COL17A1 pathway promotes the formation of multilayered, transformed epithelia

Kei Kozawa,[1,2,4,18] Miho Sekai,[1,3,18] Kenji Ohba,[3,4] Shoko Ito,[1,3] Hiroaki Sako,[1,3] Takeshi Maruyama,[3,4] Mai Kakeno,[3,4] Takanobu Shirai,[1,4] Keisuke Kuromiya,[1,4] Tomoko Kamasaki,[4] Koki Kohashi,[1,4] Shinya Tanaka,[4] Susumu Ishikawa,[4] Nanami Sato,[1,4] Shota Asano,[1] Hironori Suzuki,[1] Nobuyuki Tanimura,[1,4] Yohei Mukai,[3] Noriko Gotoh,[5] Mishie Tanino,[6,7] Shinya Tanaka,[6,7] Ken Natsuga,[8] Tomoyoshi Soga,[9] Tomonori Nakamura,[10,11] Yukihiro Yabuta,[10,11] Mitinori Saitou,[10,11,12] Takahiro Ito,[13] Kenkyo Matsuura,[13] Makoto Tsunoda,[14] Toyone Kikumori,[15] Tadashi Iida,[16] Yasuyuki Mizutani,[16] Yuki Miyai,[16] Kozo Kaibuchi,[2,17] Atsushi Enomoto,[16] and Yasuyuki Fujita[1,4,19,*]

[1]Department of Molecular Oncology, Kyoto University Graduate School of Medicine, Kyoto, Japan
[2]Department of Cell Pharmacology, Nagoya University Graduate School of Medicine, Nagoya, Japan
[3]KAN Research Institute, Inc., Kobe, Japan
[4]Division of Molecular Oncology, Institute for Genetic Medicine, Hokkaido University Graduate School of Chemical Sciences and Engineering, Sapporo, Japan
[5]Division of Cancer Cell Biology, Cancer Research Institute, Kanazawa University, Kanazawa, Japan
[6]Department of Cancer Pathology, Faculty of Medicine, Hokkaido University, Sapporo, Japan
[7]Institute for Chemical Reaction Design and Discovery (WPI-ICReDD), Hokkaido University, Sapporo, Japan
[8]Department of Dermatology, Hokkaido University Graduate School of Medicine, Sapporo, Japan
[9]Institute for Advanced Biosciences, Keio University, Tsuruoka, Japan
[10]Institute for the Advanced Study of Human Biology (WPI-ASHBi), Kyoto University, Kyoto, Japan
[11]Department of Anatomy and Cell Biology, Graduate School of Medicine, Kyoto University, Kyoto, Japan
[12]Center for iPS Cell Research and Application (CiRA), Kyoto University, Kyoto, Japan
[13]Division of Cell Fate Dynamics and Therapeutics, Department of Biosystems Science, Institute for Frontier Life and Medical Sciences, Kyoto University, Kyoto, Japan
[14]Graduate School of Pharmaceutical Sciences, The University of Tokyo, Tokyo, Japan
[15]Department of Breast and Endocrine Surgery (Surgery II), Nagoya University Graduate School of Medicine, Nagoya, Japan
[16]Department of Pathology, Nagoya University Graduate School of Medicine, Nagoya, Japan
[17]Institute for Comprehensive Medical Science (ICMS), Fujita Health University, Toyoake, Japan
[18]These authors contributed equally
[19]Lead contact
*Correspondence: fujita@monc.med.kyoto-u.ac.jp
https://doi.org/10.1016/j.cub.2021.04.078

SUMMARY

At the early stage of cancer development, oncogenic mutations often cause multilayered epithelial structures. However, the underlying molecular mechanism still remains enigmatic. By performing a series of screenings targeting plasma membrane proteins, we have found that collagen XVII (COL17A1) and CD44 accumulate in RasV12-, Src-, or ErbB2-transformed epithelial cells. In addition, the expression of COL17A1 and CD44 is also regulated by cell density and upon apical cell extrusion. We further demonstrate that the expression of COL17A1 and CD44 is profoundly upregulated at the upper layers of multilayered, transformed epithelia *in vitro* and *in vivo*. The accumulated COL17A1 and CD44 suppress mitochondrial membrane potential and reactive oxygen species (ROS) production. The diminished intracellular ROS level then promotes resistance against ferroptosis-mediated cell death upon cell extrusion, thereby positively regulating the formation of multilayered structures. To further understand the functional role of COL17A1, we performed comprehensive metabolome analysis and compared intracellular metabolites between RasV12 and COL17A1-knockout RasV12 cells. The data imply that COL17A1 regulates the metabolic pathway from the GABA shunt to mitochondrial complex I through succinate, thereby suppressing the ROS production. Moreover, we demonstrate that CD44 regulates membrane accumulation of COL17A1 in multilayered structures. These results suggest that CD44 and COL17A1 are crucial regulators for the clonal expansion of transformed cells within multilayered epithelia, thus being potential targets for early diagnosis and preventive treatment for precancerous lesions.

INTRODUCTION

Various types of tumors arise from monolayered epithelia, such as pancreas, mammary gland, lung, and intestine. The transition from monolayered to multilayered structures is one of the characteristic morphological alterations, which occurs at the relatively early stage of carcinogenesis. The multilayered transformed epithelia are often observed in precancerous lesions in a variety

Please cite this article in press as: Kozawa et al., The CD44/COL17A1 pathway promotes the formation of multilayered, transformed epithelia, Current Biology (2021), https://doi.org/10.1016/j.cub.2021.04.078

of mouse cancer models and human pathological specimens.[1–5] This oncogenic process can be also manifested in cultured cells as the foci formation of transformed cells.[6] When normal epithelial cells grow and reach high density, they stop cell division, a process termed contact inhibition of proliferation (CIP).[7] In contrast, when an oncogenic mutation occurs in the epithelial monolayer, the newly emerging transformed cells continue proliferating even at high density and are apically extruded from the cell layer, eventually forming multilayered foci structures, which is called the loss of CIP phenotype. Indeed, several oncogenic mutations, such as Ras, Src, and ErbB2, can induce multilayered structural changes in epithelia.[8–10]

The transition from monolayer to multilayer can involve multiple cellular processes, including uncontrolled cell proliferation and loss of cell polarity. In addition, apical cell extrusion is another crucial process that can potentially trigger the formation of multilayered epithelia. Upon apical extrusion, cells are exposed to distinct chemical and physical surroundings. For instance, the detachment from basement membranes leads to loss of integrin-based cell survival signals and elevation of reactive oxygen species (ROS).[11,12] In the apical lumen, cells are subject to increased shear stress by the flow of several substances, such as urine and stool. The release from the compacted epithelial layer would alter the static pressure of plasma membranes. Under such harsher conditions, apically extruded cells are often destined to death; cell death mediated by detachment from the basal substratum is termed "anoikis."[13] However, it still remains elusive how oncogenically mutated cells circumvent anoikis after apical cell extrusion, eventually leading to multilayered, transformed epithelia.

CD44 is a single-transmembrane glycoprotein. The role for CD44 at the late stage of carcinogenesis has been demonstrated by a number of studies; CD44 expression is often upregulated, playing positive roles in tumor invasion and metastasis.[14,15] The expression of CD44 is also increased at the premalignant stage in multiple types of epithelial tissues.[16–19] However, its role at the early stage of carcinogenesis remains largely unknown, though a previous study suggested that CD44 acts as a regulator for CIP.[20] COL17A1 is a type-II, single-transmembrane protein. In multilayered epithelial tissues, such as skin, COL17A1 is mainly expressed in epithelial cells at the basal layer and involved in the formation of the hemidesmosomes that anchored to the underlying basement membrane.[21] In contrast, it has not been explored whether and how COL17A1 plays a role in monolayered epithelial tissues.

In this study, we demonstrate that CD44 and COL17A1 positively regulate the formation of multilayered, transformed epithelia by enhancing resistance against cell death after apical cell extrusion.

RESULTS

Expression of RasV12 promotes the membrane accumulation of COL17A1

To identify membrane proteins of which membrane localization is promoted in transformed cells, we performed phage antibody display screening using normal and RasV12-transformed Madin-Darby canine kidney (MDCK) epithelial cells (Figure S1A). After a series of screenings, we obtained two hit antibody clones, 1C10 and 20C5, which preferentially recognized RasV12-expressing cells to normal cells (Figure 1A). Immunoblotting analyses demonstrated that both 1C10 and 20C5 antibodies recognized a protein with a size of 180 kDa, whose expression was strongly enhanced by H-RasV12 or K-RasV12 (Figure 1B). Immunoprecipitation with 1C10 or 20C5 antibody and mass spectrometric analysis revealed that either 20C5 or 1C10 binds to the identical protein, COL17A1 (Figure 1C, arrowhead). COL17A1 is a type-II membrane protein with a single-transmembrane domain (Figure 1D). Using the commercially available COL17A1 antibody, we confirmed that RasV12 expression induced the accumulation of COL17A1 at the plasma membrane in MDCK cells (Figure S1B). The upregulated COL17A1 expression by RasV12 was also observed in human pancreatic duct epithelial cells (Figure S1C). In addition, we established COL17A1-knockout cell lines and further confirmed that the hit clone antibody recognizes the COL17A1 protein (Figures S1D–S1F). Collectively, these data indicate that expression of RasV12 enhances the expression and membrane accumulation of COL17A1 in epithelial cells.

Oncogenic transformation, cell density, or cell extrusion influences COL17A1 expression

We further examined how RasV12 upregulates the expression of COL17A1. The mitogen-activated protein kinase (MAPK) and phosphatidylinositol 3-kinase (PI3K) pathways are the major downstream targets of Ras. We found that either the mitogen-activated protein kinase kinase (MEK) inhibitor U0126 or the PI3K inhibitor LY294002 canceled the RasV12-mediated upregulation of COL17A1 (Figure S2A), suggesting the involvement of the MAPK and PI3K pathways. The COL17A mRNA level was not substantially altered by RasV12 expression (Figure S2B). By blocking protein synthesis with cycloheximide, we showed that the COL17A1 proteins were profoundly stabilized by RasV12 expression (Figure S2C). Treatment with the lysosomal inhibitor chloroquine, the proteasome inhibitor MG132, or the MMP inhibitor Marimastat did not affect the expression level of COL17A1 proteins (data not shown). These results suggest that RasV12 regulates the expression of COL17A1 at a post-translational level by the major degradation machinery-independent mechanisms.

Next, we explored whether other types of transformation induce the accumulation of COL17A1. The expression of the oncogenic mutant form of Src or ErbB2 substantially increased the membrane localization of COL17A1, whereas the expression of Rap1V12, a constitutively active form of the Ras-related, non-oncogenic small guanosine triphosphatase (GTPase), did not (Figure 2A). The expression of either oncogenic mutant, Ras, Src, or ErbB2 can induce the loss of CIP phenotype, leading to multilayered epithelial structures.[22–24] Thus, we examined whether COL17A1 is involved in this oncogenic process. In normal cells, the expression of COL17A1 profoundly decreased as cells were subjected to compaction at the high-density condition (Figures 2B–2D). In RasV12-transformed cells, the cell-density-dependent regulation of COL17A1 was also moderately observed, though the expression level was higher than normal cells (Figures 2B–2D). Moreover, the increased membrane accumulation of COL17A1 was also observed in RasV12-transformed cells undergoing apical extrusion from the transformed epithelial layer (Figures 2E and 2F). We further examined whether COL17A1 is regulated upon crowding-induced cell

Please cite this article in press as: Kozawa et al., The CD44/COL17A1 pathway promotes the formation of multilayered, transformed epithelia, Current Biology (2021), https://doi.org/10.1016/j.cub.2021.04.078

CellPress

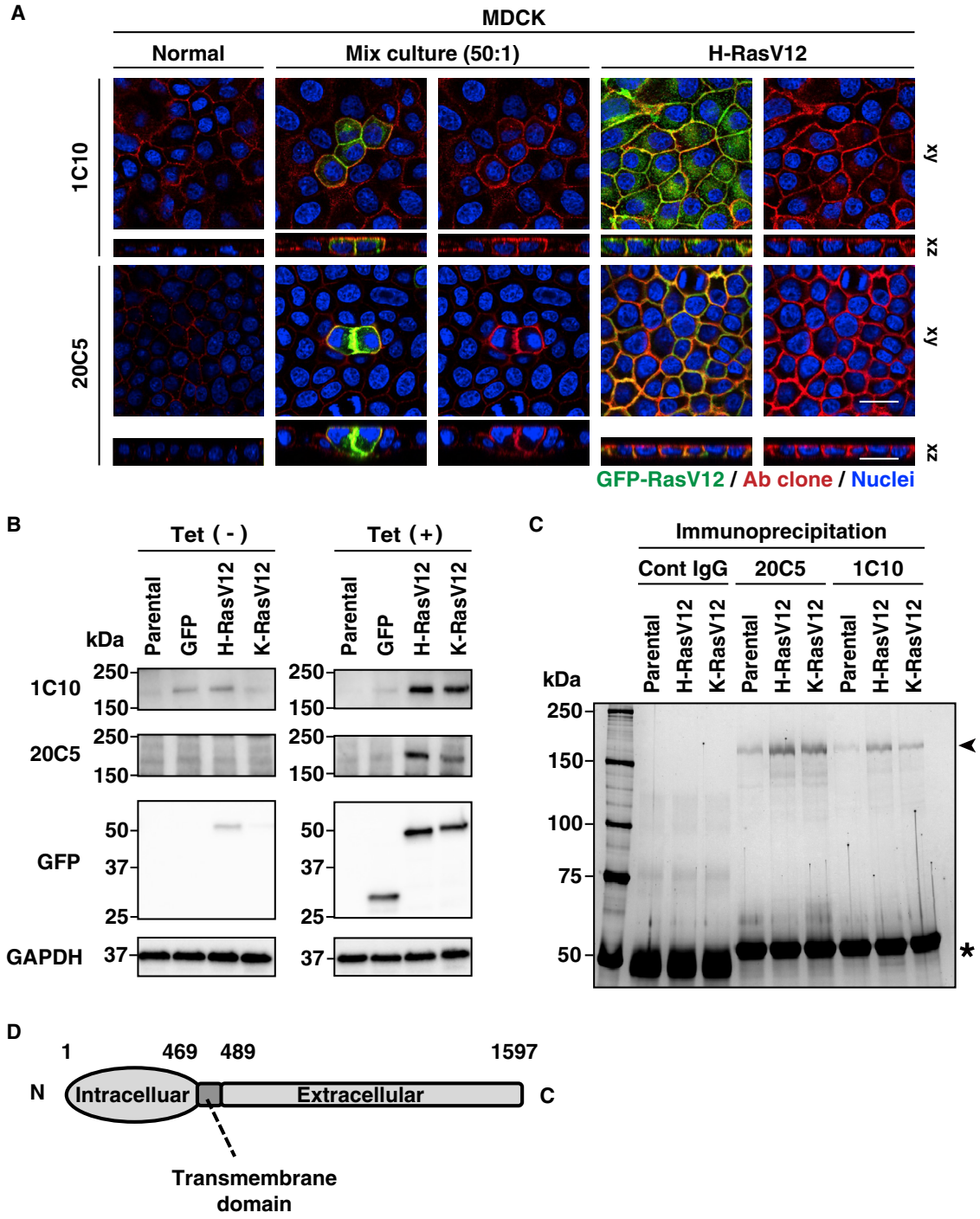

Figure 1. Expression of RasV12 promotes the membrane accumulation of COL17A1

(A) Immunofluorescence images of clone 1C10 and 20C5 antibody staining. MDCK cells were cultured alone or co-cultured with tetracycline-inducible MDCK-pTR GFP-H-RasV12 cells at a ratio of 50:1, or MDCK-pTR GFP-H-RasV12 cells were cultured alone. Cells were stained with 1C10 or 20C5 antibody (red) and Hoechst (blue). Scale bars, 20 μm. The presented images are representative from four independent experiments.

(B) Western blotting analysis with clone 1C10 or 20C5 antibody. Cell lysates from parental MDCK-pTR, MDCK-pTR GFP, MDCK-pTR GFP-H-RasV12, or MDCK-pTR GFP-K-RasV12 cells were examined.

(C) Silver staining of immunoprecipitated proteins with clone 1C10 or 20C5 antibody. The arrowhead and asterisk indicate the band for COL17A1 and heavy chains of immunoglobulin G (IgG), respectively.

(D) A schematic for the domain structure of COL17A1. The amino acid numbers correspond to the canine COL17A1 protein.

See also Figure S1.

Please cite this article in press as: Kozawa et al., The CD44/COL17A1 pathway promotes the formation of multilayered, transformed epithelia, Current Biology (2021), https://doi.org/10.1016/j.cub.2021.04.078

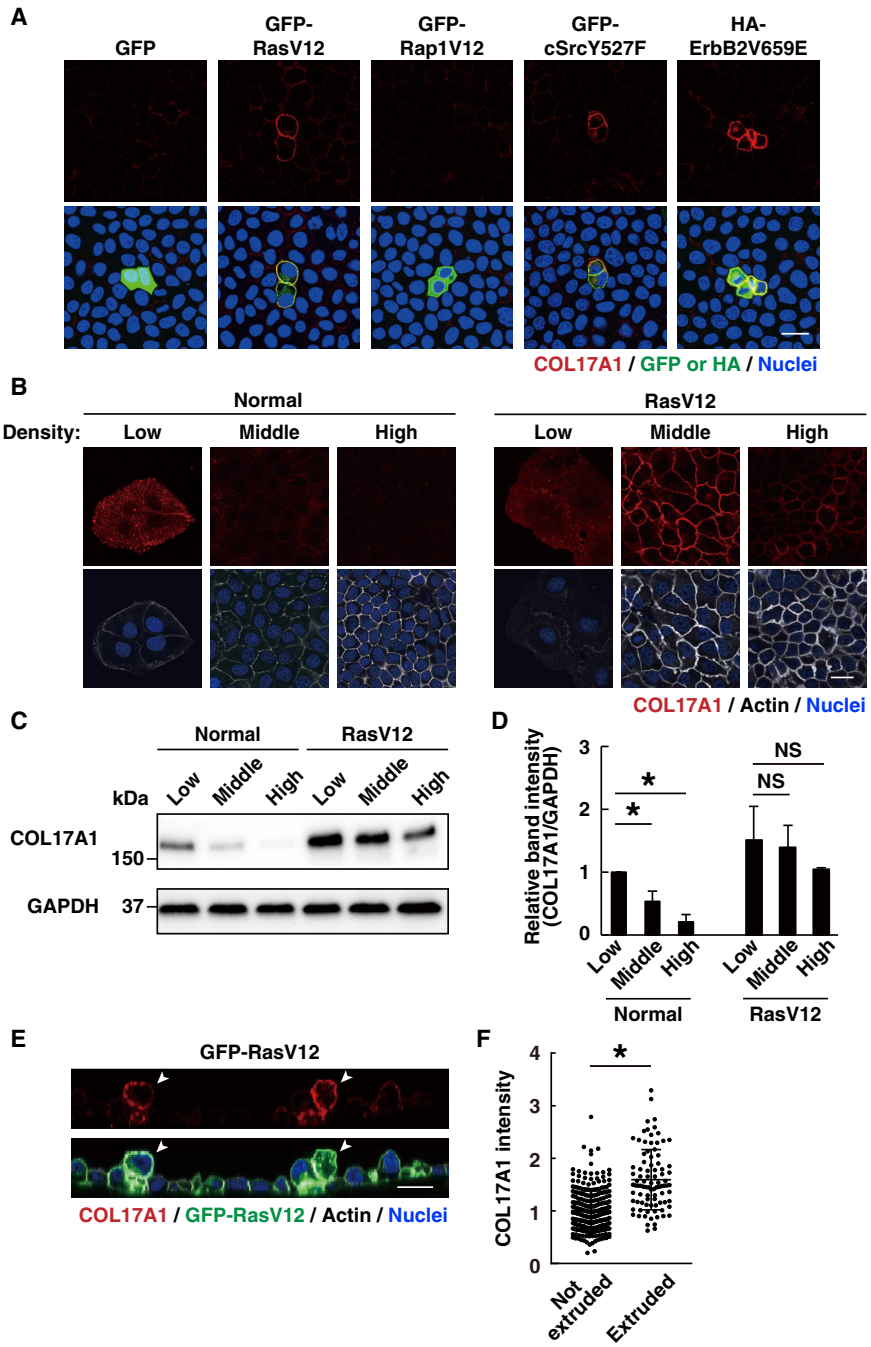

Figure 2. Oncogenic transformation, cell density, or cell extrusion influences COL17A1 expression

(A) The expression of COL17A1 in various types of transformed cells. GFP, GFP-RasV12, GFP-Rap1V12, GFP-cSrcY527F, or HA-ErbB2V659E was transiently expressed in the monolayer of normal MDCK cells, followed by immunofluorescence with anti-COL17A1 (20C5) antibody (red) and Hoechst (blue).

(B–D) Cell-density-dependent regulation of COL17A1 in normal and RasV12-transformed cells.

(B) Normal MDCK or MDCK-pTR GFP-RasV12 cells were cultured at low, middle, or high density and examined by immunofluorescence with anti-COL17A1 (20C5) antibody (red), Alexa Fluor 647-phalloidin (gray), and Hoechst (blue). The presented images are representative from three (A) or six (B) independent experiments.

(C and D) Cell lysates were examined by western blotting with anti-COL17A1 antibody.

(D) Quantification of the band intensity of COL17A1. Values are expressed as a ratio relative to normal cells at low cell density. Data are mean ± SD from three independent experiments. *$p < 0.05$ (paired two-tailed Student's t tests). NS, not significant.

(E) Immunofluorescence images of xz sections of MDCK-pTR GFP-RasV12 cells undergoing extrusion. MDCK-pTR GFP-RasV12 cells were cultured for 24 h and stained with anti-COL17A1 (20C5) antibody (red), Alexa Fluor 647-phalloidin (gray), and Hoechst (blue). The arrowheads indicate extruded cells.

(F) Quantification of COL17A1 fluorescence intensity in not extruded or extruded RasV12-transformed cells. Values are expressed as a ratio relative to not-extruded cells. Data are mean ± SD from all analyzed cells. *$p < 0.05$ (Mann-Whitney test); n = 270, 90 cells from three independent experiments.

(A, B, and E) Scale bars, 20 μm. Note that, in this study, H-Ras was used for RasV12-transformed cells if not indicated. See also Figure S2.

extrusion.[25,26] When compaction forces were applied to the monolayer of RasV12 cells cultured on the stretchable PDMS membrane, the frequency of apical cell extrusion was profoundly promoted, demonstrating the occurrence of crowding-induced cell extrusion (Figure S2D). Moreover, under the compacted condition, membrane localization of COL17A1 was substantially elevated in extruded cells (Figures S2E and S2F), suggesting that crowding-induced cell extrusion induces COL17A1 accumulation. Taken together, these data indicate that cell density and cell extrusion can regulate COL17A1.

Increased expression of COL17A1 in transformed cells plays a positive role in the formation of multilayered epithelial structures

We then explored whether COL17A1 is involved in the formation of multilayered structures in transformed epithelia. When cultured for longer times (48 h), normal epithelial cells increased cell density but still kept a monolayer where COL17A1 expression was only weakly observed (Figures 3A–3C and S3C). In contrast, RasV12-transformed cells formed multilayered, often more than three-layered, structures (Figures 3A–3C and S3C). In the multilayered regions, expression of COL17A1 was strongly enhanced in the upper layers of RasV12 cells (Figure 3A). Similarly, upregulation of COL17A1 was also observed within Src- or ErbB2-transformed, multilayered epithelia (Figure S3A). During carcinogenesis, the formation

Please cite this article in press as: Kozawa et al., The CD44/COL17A1 pathway promotes the formation of multilayered, transformed epithelia, Current Biology (2021), https://doi.org/10.1016/j.cub.2021.04.078

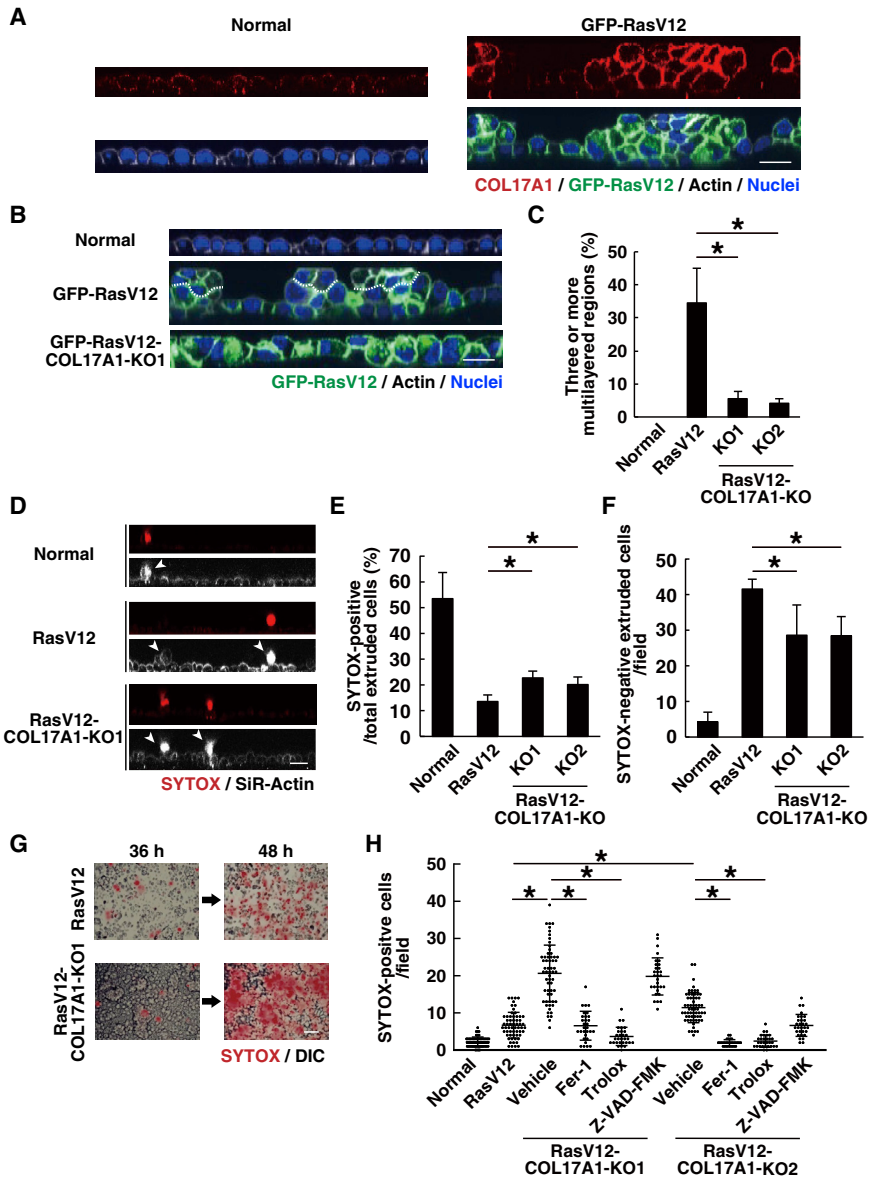

Figure 3. Increased expression of COL17A1 in transformed cells plays a positive role in the formation of multilayered epithelial structures

(A) Immunofluorescence images of COL17A1 in the multilayered, RasV12-transformed epithelium. Normal MDCK or MDCK-pTR GFP-RasV12 cells were cultured for 48 h, followed by immunofluorescence with anti-COL17A1 (20C5) antibody (red), Alexa Fluor 647-phalloidin (gray), and Hoechst (blue).

(B and C) Effect of COL17A1 knockout on the multilayered structures of RasV12-transfromed cells.

(B) Normal MDCK, MDCK-pTR GFP-RasV12 cells, or MDCK-pTRE3G GFP-RasV12 COL17A1-knockout cells were cultured for 48 h, followed by immunofluorescence with Alexa Fluor 647-phalloidin (gray) and Hoechst (blue). The dotted lines delineate the border between the second and third cell layers.

(C) Quantification of three or more multilayered regions. Data are mean ± SD from three independent experiments. *$p < 0.05$ (paired two-tailed Student's t tests). n = 15 xz images from 5 randomly selected fields (212 × 212 μm) for each cell type in each experiment.

(D–F) Effect of COL17A1 knockout on cell death after apical extrusion.

(D) The xz-immunofluorescence images of SYTOX-stained, extruded cells from the epithelial layer. Cells were cultured for 12 h and, after staining with SYTOX (red) and SiR-Actin probe (gray), further incubated for 12 h. The arrowheads indicate extruded cells.

(E) Quantification of the SYTOX-positive ratio in extruded cells. Data are mean ± SD from four independent experiments. *$p < 0.05$ (paired two-tailed Student's t tests). n = 5 fields (317 × 317 μm) for each cell type in each experiment.

(F) Quantification of the number of SYTOX-negative extruded cells. The number of SYTOX-negative extruded cells from the cell layer was analyzed in randomly selected fields (317 × 317 μm). Data are mean ± SD from four independent experiments. *$p < 0.05$ (paired two-tailed Student's t tests). n = 5 fields for each cell type in each experiment.

(G) Effect of COL17A1 knockout in RasV12-transformed MDCK cells on the SYTOX-positive cell number in the upper layers of multilayered epithelia. GFP-RasV12 or GFP-RasV12 COL17A1-knockout cells were cultured for the indicated times. Cells were analyzed by SYTOX (red) and phase contrast (differential interference contrast [DIC]). Images are extracted from a representative time-lapse analysis.

(H) Effect of the ferroptosis inhibitor Fer-1, the ROS scavenger Trolox, or the apoptosis inhibitor Z-VAD-FMK on the number of SYTOX-positive cells. Normal, RasV12, or RasV12 COL17A1-knockout cells were cultured for 48 h in the absence or presence of the inhibitor. The ratio of SYTOX-positive cells at the upper layers was analyzed in randomly selected fields (2,048 × 2,048 pixels). Data are mean ± SD from all analyzed fields. n = 10 fields for each analysis in six (normal, RasV12, and vehicle) or three (Fer-1, Trolox, and Z-VAD-FMK) independent experiments. *$p < 0.05$ (one-way ANOVA with Tukey's test).

(A, B, and D) Scale bars, 20 μm. (G) Scale bar, 100 μm. The presented images are representative of more than ten (A) or five (G) independent experiments. See also Figure S3.

of multilayered structures can be observed at the early precancerous stage in various epithelial tissues, including PanIN (pancreatic intraepithelial neoplasia) lesions in the pancreas.[27] We thus examined whether COL17A1 expression is upregulated in multilayered, precancerous lesions in the KPC mice. KPC is a pancreatic cancer mouse model where mutations in *K-Ras* and *p53* genes are induced in pancreatic ductal epithelia.[3] At postnatal 8–10 weeks, PanIN-like precancerous lesions are frequently observed within the lumen of pancreatic epithelial ducts. In the wild-type mice, COL17A1 expression was not clearly observed within the monolayer of a pancreatic ductal epithelium (Figure S3B). In contrast, in the KPC mice, expression of COL17A1 was increased in some of the multilayered precancerous lesions (Figure S3B). These data imply that expression of COL17A1 is upregulated in multilayered precancerous lesions *in vivo* as well. To investigate the functional involvement of

Please cite this article in press as: Kozawa et al., The CD44/COL17A1 pathway promotes the formation of multilayered, transformed epithelia, Current Biology (2021), https://doi.org/10.1016/j.cub.2021.04.078

COL17A1 in the formation of multilayered structures, we examined the effect of COL17A1 knockout in RasV12-transformed cells. We found that the formation of multilayered structures was substantially suppressed in COL17A1-knockout RasV12 epithelia; more than three-layered structures were not frequently observed, compared with RasV12-transformed epithelia (Figures 3B, 3C, and S3C), indicating that COL17A1 plays a crucial role in the formation of multilayered, transformed epithelia.

The organization of multilayered lesions is frequently observed in monolayered epithelial tissues during cancer development.[1–5] The formation and maintenance of multilayered epithelial structures can involve multiple underlying molecular mechanisms: (1) uncontrolled cell proliferation; (2) loss of cell polarity; (3) misoriented spindle formation during mitosis; (4) enhanced crowding-induced cell extrusion; and (5) resistance against anoikis. We then analyzed whether these processes are influenced by the expression of RasV12 or COL17A1. EdU incorporation was promoted by RasV12 expression, which was not substantially affected by COL17A1 knockout (Figure S3D). Localization of cell polarity markers was not affected by RasV12 expression or COL17A1 knockout (Figure S3E). In addition, spindle orientation was not disrupted by RasV12 expression or COL17A1 knockout (Figure S3F). Next, we examined the frequency of apical cell extrusion and the following cell death. We first analyzed the apical extrusion from the epithelial monolayer that reached high density after 24 h of plating. Under the crowded condition, RasV12 cells were more frequently extruded than normal cells, but the number of extruded COL17A1-knockout RasV12 cells was comparable to that of extruded RasV12 cells (Figures S3G and S3H). We further analyzed the occurrence of cell death upon apical extrusion using the cell death fluorescence-indicator SYTOX. Nearly half of extruded normal cells were stained with SYTOX, indicating cell death, whereas only 10% of extruded RasV12 cells were SYTOX positive (Figures 3D and 3E). COL17A1 knockout in RasV12 cells significantly elevated the death ratio of extruded cells (Figures 3D and 3E) and substantially diminished the appearance of SYTOX-negative (alive) extruded RasV12-transformed cells from the monolayer (Figure 3F). To further elucidate the role for COL17A1 in the maintenance of multilayered epithelial structures, we examined SYTOX staining where RasV12 cells had formed multilayered regions after 48 h of plating. COL17A1 knockout in RasV12 cells profoundly increased the number of SYTOX-positive cells in the upper layers of multilayered epithelia (Figures 3G and 3H). In contrast, COL17A1 knockout in normal cells did not induce cell death (Figure S3I). Collectively, these data indicate that COL17A1 positively regulates the formation and maintenance of multilayered transformed epithelia by suppressing extrusion-induced cell death. It should be noted that the number of extruded COL17A1-knockout RasV12 cells shown in Figure S3H could be underestimated because of the increased cell death upon cell extrusion; we cannot thus exclude the possibility that apical extrusion is upregulated by COL17A1 knockout in transformed epithelia.

Cells that have been detached from the basal substratum are destined to death via apoptosis or ferroptosis.[11,28] We found that the ferroptosis inhibitor ferrostatin (Fer)-1 strongly suppressed the number of SYTOX-positive COL17A1-knockout RasV12 cells at the upper layers of multilayered epithelia, although the apoptosis inhibitor Z-VAD-FMK had only moderate effect (Figure 3H). Ferroptosis is caused by accumulation of peroxidized lipids. Indeed, the ROS scavenger Trolox profoundly suppressed the death ratio of COL17A1-knockout RasV12 cells (Figure 3H), suggesting that COL17A1 suppresses ROS-mediated ferroptosis during the formation of multilayered structures.

COL17A1 negatively regulates mitochondrial membrane potential, thereby suppressing the production of ROS

Next, we explored molecular mechanisms whereby COL17A1 regulates the ROS-mediated cell death. C11-BODIPY acts as a fluorescent proxy for radical-mediated lipid peroxidation.[29] We found that, under the monolayered culture conditions, COL17A1 knockout in RasV12 cells substantially elevated cytoplasmic C11-BODIPY staining (Figure 4A), which was suppressed by the lipophilic antioxidant Fer-1 (Figure S4A), suggesting that COL17A1 suppresses lipid peroxidation within the monolayered, transformed epithelium, even prior to the formation of multilayered structures. Mitochondria are one of the major sources for ROS production. Using MitoSOX, an indicator for mitochondrial superoxide production, we demonstrated that COL17A1 knockout in RasV12 cells significantly promoted MitoSOX fluorescence intensity (Figures 4B and 4C). TMRM (tetramethylrhodamine methyl ester) is a positively charged red fluorescent dye that is incorporated into mitochondria according to the membrane potential gradient across their inner membranes. We found that the TMRM fluorescence was strongly increased in COL17A1-knockout RasV12 cells (Figures 4D and 4E). The TMRM fluorescence was suppressed in the upper layers within multilayered RasV12 epithelia although promoted in COL17A1-knockout RasV12 epithelia (Figure 4F). CCCP (carbonyl cyanide m-chlorophenyl hydrazone) is a mitochondrial oxidative phosphorylation uncoupler, which reduces mitochondrial membrane potential. The treatment of CCCP strongly suppressed the C11-BODIPY, MitoSOX, and TMRM intensities in COL17A1-knockout RasV12 cells (Figures 4A–4E), indicating that the increased mitochondrial membrane potential results in the ROS production.

To further analyze the effect of COL17A1 knockout on metabolic pathways, we performed comprehensive metabolome analysis and compared intracellular metabolites between RasV12 and COL17A1-knockout RasV12 cells (the whole metabolome analysis data are shown at https://molonc.researcherinfo.net/metabolome1.pdf). In COL17A1-knockout RasV12 cells, the amounts of a battery of metabolites in the TCA cycle decreased, whereas the level of succinate was upregulated (Figures S4B and S4F). Incorporation of glucose analog 2-NBDG or the level of antioxidant glutathione was not altered in COL17A1-knockout RasV12 cells (Figures S4C and S4D). Succinate can be generated by the glutamate-GABA pathway (GABA shunt) in addition to the TCA cycle (Figure S4F).[30] In COL17A1-knockout RasV12 cells, the level of GABA was profoundly suppressed and the mRNA levels of glutamate decarboxylase 2 (GAD2) and 4-aminobutyrate aminotransferase (ABAT) were significantly increased (Figures S4B, S4E, and S4F), suggesting that the production of succinate is elevated through the GABA shunt pathway. Despite the increased TMRM, the ATP level was decreased in COL17A1-knockout RasV12 cells (Figure S4B). Furthermore, treatment with rotenone, a selective inhibitor for mitochondrial complex I,

Please cite this article in press as: Kozawa et al., The CD44/COL17A1 pathway promotes the formation of multilayered, transformed epithelia, Current Biology (2021), https://doi.org/10.1016/j.cub.2021.04.078

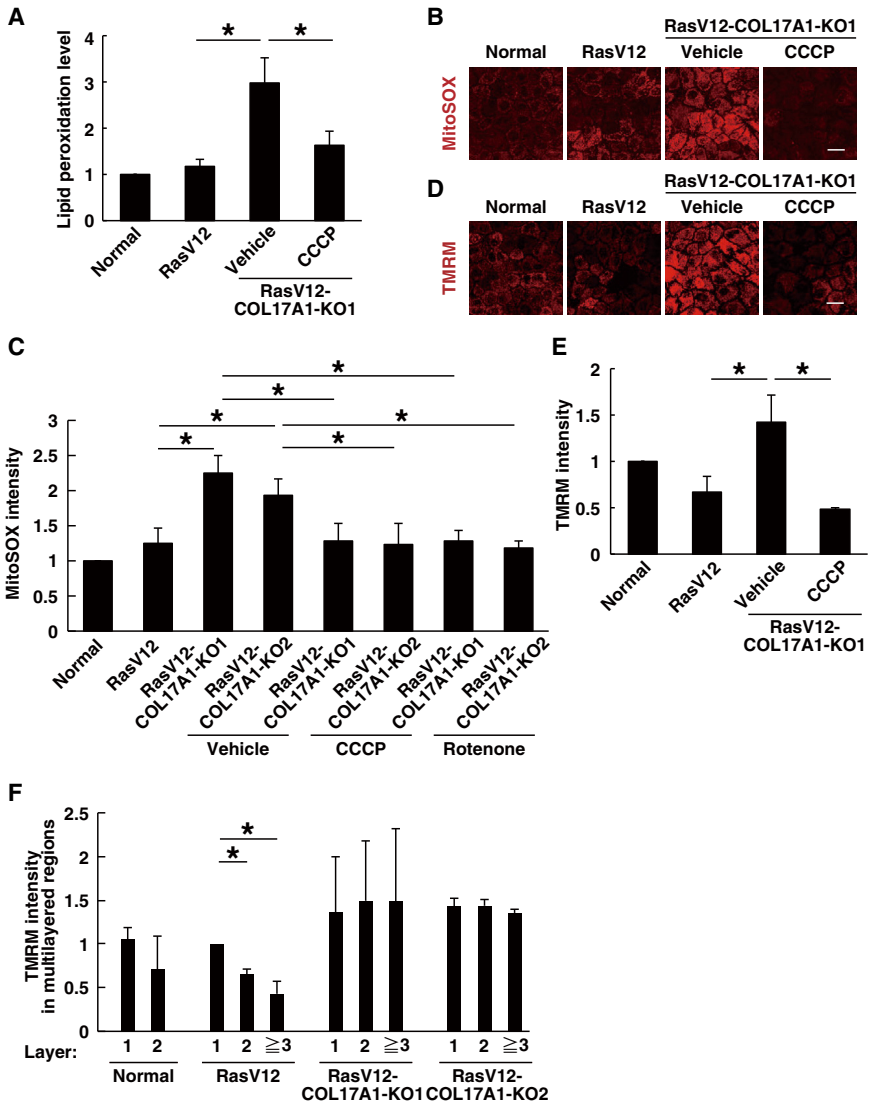

Figure 4. COL17A1 negatively regulates mitochondrial membrane potential, thereby suppressing the production of ROS

(A) Effect of COL17A1 knockout in RasV12-transformed cells on the level of intracellular lipid peroxidation. Normal MDCK, MDCK-pTRE3G Myc-RasV12, or MDCK-pTRE3G Myc-RasV12 COL17A1-knockout cells were cultured for 24 h in the absence or presence of CCCP, followed by incubation with C11-BODIPY. The level of lipid peroxidation was assessed by the ratio of oxidized to non-oxidized C11-BODIPY staining. Values are expressed as a ratio relative to normal cells. Data are mean ± SD from three independent experiments. *p < 0.05 (paired two-tailed Student's t tests); n = 417, 362, 394, and 349 cells.

(B and C) Effect of COL17A1 knockout on the production of mitochondrial superoxide. Cells were cultured for 24 h in the absence or presence of CCCP or rotenone, followed by staining with MitoSOX (red).

(C) Quantification of the fluorescence intensity of MitoSOX. Values are expressed as a ratio relative to normal cells. Data are mean ± SD from seven (normal, RasV12, and vehicle), four (CCCP), or three (rotenone) independent experiments. *p < 0.05 (unpaired two-tailed Student's t tests); n = 916, 834, 875, 865, 420, 438, 157, and 166 cells.

(D and E) Effect of COL17A1 knockout on the mitochondrial membrane potential. Cells were cultured for 24 h in the absence or presence of CCCP, followed by staining with TMRM (red).

(B and D) Scale bars, 20 μm.

(E) Values are expressed as a ratio relative to normal cells. Data are mean ± SD from three (normal, RasV12, and vehicle) or two (CCCP) independent experiments. *p < 0.05 (unpaired two-tailed Student's t tests); n = 379, 309, 309, and 203 cells.

(F) Quantification of the fluorescence intensity of TMRM in multilayered regions. Cells were cultured for 48 h, followed by staining with TMRM. Values are expressed as a ratio relative to RasV12 cells in the first layer. Data are mean ± SD from three (RasV12 and RasV12-COL17A1-KO1) or two (normal and RasV12-COL17A-KO2) independent experiments. n = 197, 3, 345, 187, 66, 287, 105, 9, 184, 113, and 12 cells. *p < 0.05 (unpaired two-tailed Student's t tests).

See also Figure S4.

diminished the MitoSOX intensity in COL17A1-knockout RasV12 cells (Figure 4C). Collectively, these data imply that COL17A1 knockout might promote the generation of ROS by the reverse electron transport in the mitochondrial complex I, accompanied by the increased succinate level (Figure S4F).[31,32]

CD44 regulates membrane accumulation of COL17A1 in multilayered epithelia

By another screening approach with Cell Surface Marker Screening Panel (BD Biosciences), we identified CD44 as another membrane protein whose membrane localization was promoted by RasV12 expression (M. Sekai, unpublished data). It has been also reported by other groups that RasV12 expression induces the upregulation of CD44.[33,34] Using MDCK epithelial cells, we demonstrated that expression of RasV12 or Src, but not Rap1V12, enhanced the membrane localization of CD44 at the cell-cell adhesion sites (Figure 5A). CD44 has been reported to be involved in CIP.[20] In normal cells, expression of CD44 was diminished at the high-density condition, whereas in RasV12 cells, the cell-density-dependent regulation of CD44 was only moderately observed (Figure S5A). Thus, expression of CD44 can be regulated by expression of oncogenic mutants or cell density, similarly to that of COL17A1. Indeed, CD44 expression was prominently promoted in RasV12- or Src-transformed multilayered epithelia (Figures 5B and S5B). The expression of CD44 was also profoundly elevated in the multilayered PanIN-like lesions in the pancreas of KPC mice (Figure S5C). Moreover, knockdown of CD44 in RasV12 cells significantly decreased the formation of multilayer regions (Figures 5B and 5C). CD44 knockdown did not significantly

Please cite this article in press as: Kozawa et al., The CD44/COL17A1 pathway promotes the formation of multilayered, transformed epithelia, Current Biology (2021), https://doi.org/10.1016/j.cub.2021.04.078

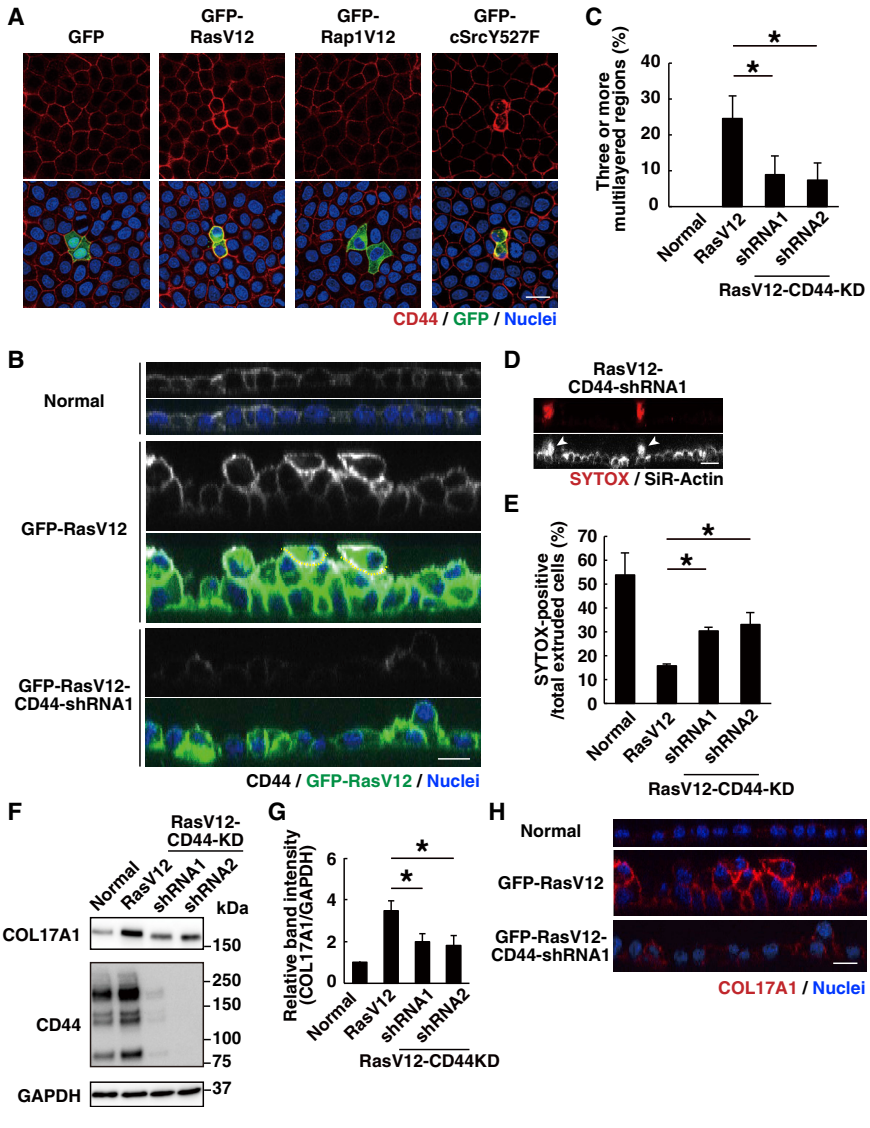

Figure 5. CD44 regulates membrane accumulation of COL17A1 in multilayered epithelia

(A) The expression of CD44 in various types of transformed cells. GFP, GFP-RasV12, GFP-Rap1V12, or GFP-cSrcY527F was transiently expressed in the monolayer of normal MDCK cells, followed by immunofluorescence with anti-CD44 antibody (red) and Hoechst (blue).

(B) Immunofluorescence images of CD44 in multilayered, transformed epithelia. Normal MDCK, MDCK-pTR GFP-RasV12, or MDCK-pTR GFP-RasV12 CD44-shRNA cells were cultured for 48 h, followed by immunofluorescence with anti-CD44 antibody (gray) and Hoechst (blue). The dotted lines delineate the border between the second and third cell layers.

(C) Quantification of three or more multilayered regions. Data are mean ± SD from three independent experiments. *$p < 0.05$ (paired two-tailed Student's t tests). n = 15 xz-images from 5 randomly selected fields (212 × 212 μm) for each cell type in each experiment.

(D) The xz-immunofluorescence images of SYTOX-stained, extruded cells from the epithelial layer. CD44-knockdown GFP-RasV12 cells were cultured for 12 h, and after staining with SYTOX (red) and SiR-actin probe (gray), cells were further incubated for 12 h. The arrowheads indicate extruded cells.

(E) Effect of CD44 knockdown on the SYTOX-positive ratio in extruded cells. Data are mean ± SD from three independent experiments. *$p < 0.05$ (paired two-tailed Student's t tests). n = 152, 603, 636, and 512 cells from 15 randomly selected fields (317 × 317 μm).

(F and G) Effect of CD44 knockdown on COL17A1 expression. Cell lysates from the indicated cells were examined by western blotting with anti-COL17A1 or anti-CD44 antibody.

(G) Quantification of the band intensity of COL17A1. Values are expressed as a ratio relative to normal cells. Data are mean ± SD from three independent experiments. *$p < 0.05$ (paired two-tailed Student's t tests).

(H) Effect of CD44 knockdown on COL17A1 expression in the multilayered RasV12 cells. Cells were cultured for 48 h, followed by immunofluorescence with anti-COL17A1 (20C5) antibody (red) and Hoechst (blue). The same samples as (B) were used for the anti-COL17A1 immunofluorescence analysis.

(A, B, D, and H) Scale bars, 20 μm. The presented images are representative from more than three (A) or four (B and H) independent experiments. See also Figure S5.

affect cell proliferation, cell polarity, or spindle orientation during mitosis (Figures S5D–S5F). In contrast, CD44 knockdown substantially elevated the SYTOX-positive ratio of RasV12 cells undergoing apical cell extrusion (Figures 5D and 5E), demonstrating that CD44 and COL17A1 play a comparable role in the formation of multilayered structures in transformed epithelia. In addition, CD44 knockdown in RasV12 cells elevated the MitoSOX and TMRM intensities, which were diminished by CCCP (Figures S5G and S5H). We also demonstrated that CD44 knockdown in RasV12-transformed cells substantially suppressed the upregulated expression and membrane accumulation of COL17A1 in multilayered epithelia (Figures 5F–5H). COL17A1 knockout in RasV12 cells suppressed CD44 expression but did not substantially influence CD44 accumulation in multilayered epithelia (Figures S5I–S5K). Collectively, these data suggest that CD44 regulates membrane accumulation of COL17A1 in transformed, multilayered structures.

DISCUSSION

Oncogenic transformations often cause the transition from monolayered to multilayered epithelial structures at the early or middle stage of carcinogenesis prior to the acquisition of malignant phenotypes. To attain clonal expansion during cancer evolution, transformed cells need to gain sufficient space by escaping from the compacted epithelium; hence, transformed cells proceed into the apical lumen via cell extrusion, leading to the formation of multilayered epithelia. However, the apically extruded cells would be subject to various physical and chemical stresses in the new environment. For instance, in the apical

Please cite this article in press as: Kozawa et al., The CD44/COL17A1 pathway promotes the formation of multilayered, transformed epithelia, Current Biology (2021), https://doi.org/10.1016/j.cub.2021.04.078

lumen, cells are often exposed to shear stress by the flow of a variety of substances, such as urine or stool. In addition, the detachment from the basement membrane leads to loss of integrin-based survival signals. But the underlying molecular mechanisms had remained elusive how transformed cells acquire resistance against cell death under such harsher conditions. In this study, we have demonstrated that the CD44/COL17A1 pathway is involved in the formation and maintenance of transformation-mediated multilayered epithelia. CD44 and COL17A1 share several common features and functions. First, the expression of CD44 or COL17A1 is enhanced by RasV12 expression. Second, the expression of CD44 or COL17A1 can be regulated by cell density. Third, the expression of CD44 or COL17A1 is elevated in the upper layers of transformed, multilayered epithelia. Fourth, CD44 or COL17A1 plays a positive role in the formation of multilayered epithelia. Fifth, the expression of CD44 or COL17A1 suppresses the cell death after apical cell extrusion. In addition, CD44 and COL17A1 mutually regulate their expression, though immunoprecipitation analyses have not shown the physical interaction between CD44 and COL17A1 (data not shown). The increased expression of CD44 or COL17A1 is also observed in multilayered PanIN lesions in KPC mice. In contrast to the prominent accumulation of CD44 at most of RasV12-transformed, multilayered epithelia, increased expression of COL17A1 can be observed less frequently in some of the multilayered PanIN lesions. There may be certain molecular mechanisms that negatively regulate COL17A1 expression *in vivo*.

How does cell density control CD44/COL17A1 expression? A previous report has shown that CD44 is involved in CIP,[20] though the molecular mechanism remains obscure. At the upper layers in multilayered RasV12-transformed epithelia, nuclear localization of YAP/TAZ was not observed (data not shown), suggesting that the well-known regulators of CIP, YAP/TAZ,[35] are not involved in the regulation of CD44/COL17A1. The more detailed molecular mechanism of how expression of CD44/COL17A1 is regulated at multilayered epithelia needs to be clarified in future studies.

Recent studies have brought about a new concept: crowding-induced cell extrusion; at high cell density, under the compacted condition, cells can be apically extruded from a monolayer of the epithelium.[25,26] Crowding-induced cell extrusion is not merely caused by mechanical forces but can involve signaling events, such as reduced ERK signaling and caspase activation.[36,37] However, to date, crowding-induced extrusion of transformed cells has not been mechanistically linked to the formation and/or maintenance of multilayered epithelial structures. Our data in this study imply a notion that CD44/COL17A1 are crucial regulators that influence the cell fate upon crowing-induced cell extrusion, thereby modulating the formation of multilayered epithelia. The expression of CD44/COL17A1 is suppressed under the compacted, high-cell-density condition. Thus, upon crowding-induced cell extrusion, cells are released from the compacted epithelia, which would cause the elevated expression of CD44/COL17A1; the alteration in physical circumstances might regulate CD44/COL17A1 in the upper layers of multilayered epithelia. We also demonstrate that COL17A1 membrane localization is promoted when stretching forces are applied to the monolayer of normal cells cultured on the stretchable PDMS membrane (Figure S5L), further confirming the mechanical regulation of COL17A1. The knockdown of E-cadherin can induce the multilayered epithelia with frequent apoptotic events, but the level of CD44/COL17A1 was not increased at the upper layers (Figure S5M), suggesting that not only multilayered structures but also oncogenic mutations and probably other unknown factors are required for upregulation of CD44/COL17A1.

Previous studies have shown that, when RasV12-transformed cells are surrounded by normal epithelial cells, RasV12 cells are apically extruded via cell competition with the surrounding normal cells and eventually eliminated from epithelial tissues.[38–40] These results indicate that normal epithelia have anti-tumor activity that does not involve immune systems; this tumor-suppressive mechanism is termed EDAC (epithelial defense against cancer).[41] Thus, extrusion of RasV12-transformed cells in EDAC or in the formation of multilayered structures plays an opposite role, suppressing or promoting, in tumor development. One possibility is that the fate of apically extruded transformed cells can be substantially affected by the underlying cells. When RasV12-transformed cells are apically extruded from the monolayer of normal cells, the extruded RasV12 cells and the underlying normal cells just weakly adhere or tend to be segregated,[38,42] often leading to the dissociation of transformed cells into the apical lumen. In contrast, when RasV12-transformed cells are apically extruded from the monolayer of RasV12 cells, the extruded RasV12 cells maintain cell-cell adhesions with the underlying RasV12 cells and keep attaching to the epithelium. These mechanistic and functional differences highlight versatile roles of cell extrusion in cancer development.

In stratified epithelia, such as skin, the expression level of COL17A1 is high in the basal layer, especially at the hemidesmosomes, and low or none in the upper layers. In contrast, in monolayered epithelial tissues, the expression of COL17A1 is quite low and not localized at the hemidesmosomes, and as described in this study, the COL17A1 expression is substantially elevated in the upper layers within transformed, multilayered structures. These data suggest that the functional role of COL17A1 is distinct between monolayer and multilayer epithelial tissues.

By thoroughly examining the effect of COL17A1 knockout in RasV12 cells, we demonstrate that COL17A1 is involved in cellular metabolism. In COL17A1-knockout RasV12 cells, the level of ROS is upregulated. The intracellular ROS level can be regulated by the balance between the ROS production and the antioxidants-mediated reduction. A previous study has shown that expression of a splice variant of CD44 induces the higher level of glutathione whereby promoting anti-oxidation activity.[43] However, COL17A1 knockout does not affect the glutathione level (Figure S4D). So far, we have not found antioxidants of which level is profoundly affected by COL17A1 knockout. Instead, our data indicate that COL17A1 knockout promotes the production of ROS at mitochondria. In COL17A1-knockout RasV12 cells, the superoxide level and membrane potential in mitochondria are elevated. Treatment with CCCP suppresses mitochondrial superoxide, indicating that the increased mitochondrial membrane potential causes the higher level of intracellular ROS, whereby promoting cell death. A selective inhibitor for mitochondrial complex I rotenone substantially suppresses the ROS production in mitochondria (Figure 4C). Previous reports have demonstrated that the increased level of succinate and mitochondrial membrane potential can trigger the production of ROS through the reverse electron transport via mitochondrial

complex I.[31,32] Indeed, the metabolome analysis has revealed that, in COL17A1-knockout RasV12 cells, the level of succinate is elevated, whereas that of GABA is decreased, implying that COL17A1 regulates the metabolic pathway from the GABA shunt to mitochondrial complex I through succinate, thereby suppressing the ROS production (Figure S4F). In addition to the pathway from the GABA shunt to mitochondrial complex I, various metabolic changes are observed in COL17A1-knockout RasV12-transformed cells, such as elevated kynurenine and decreased tryptophan (https://molonc.researcherinfo.net/metabolome1.pdf). Hence, the molecular mechanisms of how CD44/COL17A1 regulate those cellular metabolisms are not yet fully understood, which need to be further elucidated in future studies.

Multilayered epithelial structures are observed in certain types of precancerous lesions, such as PanIN in the pancreas. During the development of pancreatic cancer, the mutation in the *Ras* gene frequently occurs at the initial stage; most of PanIN lesions carry *Ras* mutations.[44] Pancreatic cancer patients suffer from an extremely low 5-year survival rate due to the occurrence of early and frequent metastasis into distant organs.[45–47] Thus, early detection and eradication are necessary to improve the poor prognosis. We expect that CD44 would be a potential target for the establishment of early diagnosis and preventive treatment for precancerous tumors.

STAR★METHODS

Detailed methods are provided in the online version of this paper and include the following:

- KEY RESOURCES TABLE
- RESOURCE AVAILABILITY
  - Lead contact
  - Materials availability
  - Data and code availability
- EXPERIMENTAL MODEL AND SUBJECT DETAILS
- METHOD DETAILS
  - Antibodies, Plasmids, and Materials
  - Establishment of Cell Lines
  - Immunofluorescence and Western Blotting
  - Phage Antibody Display Screening
  - Immunoprecipitation and Mass Spectrometry
  - Compression or Stretching Assay
  - Quantitative Real-Time PCR
  - Mouse Pancreatic Cancer (KPC) Model and Immunohistochemistry
  - Metabolome Analysis
  - Quantification of Glutathione
- QUANTIFICATION AND STATISTICAL ANALYSIS

SUPPLEMENTAL INFORMATION

Supplemental information can be found online at https://doi.org/10.1016/j.cub.2021.04.078.

ACKNOWLEDGMENTS

We thank K. Endo and S. Ashitani (Keio University) for technically supporting metabolome analysis. We also thank K. Ushida (Nagoya University) and T. Sato (Eisai Co., Ltd.) for technical support of histopathological and mass-spectrometric analyses, respectively. This work was supported by Japan Society for the Promotion of Science (JSPS) Grant-in-Aid for Scientific Research (A) 18H03994, JST (Moonshot R&D: grant number JPMJPS2022), the Takeda Science Foundation, the Uehara Memorial Foundation, and SAN-ESU GIKEN Co., Ltd. (to Y.F.) and by the fellowship from the Takeda Science Foundation (to K. Kozawa). This work was also supported by Kyoto University Live Imaging Center.

AUTHOR CONTRIBUTIONS

K. Kozawa and M. Sekai designed experiments and generated most of the data. K.O., S. Ito, H. Sako, T.M., M.K., T. Shirai, K. Kuromiya, T. Kamasaki, K. Kohashi, Shinya Tanaka (the 12th author), S. Ishikawa, N.S., S.A., H. Suzuki, N.T., and K. Kaibuchi assisted experiments. Y. Mukai generated phage antibody libraries. N.G., M. Tanino, Shinya Tanaka (the 21st author), K.N., T. Kikumori, T. Iida, Y. Mizutani, Y. Miyai, and A.E. assisted immunohistochemistry analyses. T. Soga, T. Ito, K.M., and M. Tsunoda assisted the analyses of metabolome and metabolic pathways. T.N., Y.Y., and M. Saitou assisted RNA sequencing (RNA-seq) analysis. Y.F. conceived and designed the study. The manuscript was written by K. Kozawa, M. Sekai, and Y.F. with assistance from the other authors.

DECLARATION OF INTERESTS

The authors declare no competing interests.

Received: December 21, 2020
Revised: March 30, 2021
Accepted: April 29, 2021
Published: June 3, 2021

REFERENCES

1. Iacobuzio-Donahue, C.A., Velculescu, V.E., Wolfgang, C.L., and Hruban, R.H. (2012). Genetic basis of pancreas cancer development and progression: insights from whole-exome and whole-genome sequencing. Clin. Cancer Res. *18*, 4257–4265.
2. Hruban, R.H., Takaori, K., Klimstra, D.S., Adsay, N.V., Albores-Saavedra, J., Biankin, A.V., Biankin, S.A., Compton, C., Fukushima, N., Furukawa, T., et al. (2004). An illustrated consensus on the classification of pancreatic intraepithelial neoplasia and intraductal papillary mucinous neoplasms. Am. J. Surg. Pathol. *28*, 977–987.
3. Hingorani, S.R., Wang, L., Multani, A.S., Combs, C., Deramaudt, T.B., Hruban, R.H., Rustgi, A.K., Chang, S., and Tuveson, D.A. (2005). Trp53R172H and KrasG12D cooperate to promote chromosomal instability and widely metastatic pancreatic ductal adenocarcinoma in mice. Cancer Cell *7*, 469–483.
4. Casasent, A.K., Edgerton, M., and Navin, N.E. (2017). Genome evolution in ductal carcinoma in situ: invasion of the clones. J. Pathol. *241*, 208–218.
5. Burstein, H.J., Polyak, K., Wong, J.S., Lester, S.C., and Kaelin, C.M. (2004). Ductal carcinoma in situ of the breast. N. Engl. J. Med. *350*, 1430–1441.
6. Temin, H.M. (1960). The control of cellular morphology in embryonic cells infected with rous sarcoma virus in vitro. Virology *10*, 182–197.
7. Abercrombie, M. (1970). Contact inhibition in tissue culture. In Vitro *6*, 128–142.
8. Haigis, K.M., Kendall, K.R., Wang, Y., Cheung, A., Haigis, M.C., Glickman, J.N., Niwa-Kawakita, M., Sweet-Cordero, A., Sebolt-Leopold, J., Shannon, K.M., et al. (2008). Differential effects of oncogenic K-Ras and N-Ras on proliferation, differentiation and tumor progression in the colon. Nat. Genet. *40*, 600–608.
9. Merrick, D.T., Kittelson, J., Winterhalder, R., Kotantoulas, G., Ingeberg, S., Keith, R.L., Kennedy, T.C., Miller, Y.E., Franklin, W.A., and Hirsch, F.R. (2006). Analysis of c-ErbB1/epidermal growth factor receptor and c-ErbB2/HER-2 expression in bronchial dysplasia: evaluation of potential

Please cite this article in press as: Kozawa et al., The CD44/COL17A1 pathway promotes the formation of multilayered, transformed epithelia, Current Biology (2021), https://doi.org/10.1016/j.cub.2021.04.078

targets for chemoprevention of lung cancer. Clin. Cancer Res. *12*, 2281–2288.

10. Cordero, J.B., Ridgway, R.A., Valeri, N., Nixon, C., Frame, M.C., Muller, W.J., Vidal, M., and Sansom, O.J. (2014). c-Src drives intestinal regeneration and transformation. EMBO J. *33*, 1474–1491.
11. Frisch, S.M., and Screaton, R.A. (2001). Anoikis mechanisms. Curr. Opin. Cell Biol. *13*, 555–562.
12. Schafer, Z.T., Grassian, A.R., Song, L., Jiang, Z., Gerhart-Hines, Z., Irie, H.Y., Gao, S., Puigserver, P., and Brugge, J.S. (2009). Antioxidant and oncogene rescue of metabolic defects caused by loss of matrix attachment. Nature *461*, 109–113.
13. Frisch, S.M., and Francis, H. (1994). Disruption of epithelial cell-matrix interactions induces apoptosis. J. Cell Biol. *124*, 619–626.
14. Martin, T.A., Harrison, G., Mansel, R.E., and Jiang, W.G. (2003). The role of the CD44/ezrin complex in cancer metastasis. Crit. Rev. Oncol. Hematol. *46*, 165–186.
15. Senbanjo, L.T., and Chellaiah, M.A. (2017). CD44: a multifunctional cell surface adhesion receptor is a regulator of progression and metastasis of cancer cells. Front. Cell Dev. Biol. *5*, 18.
16. Auvinen, P., Tammi, R., Tammi, M., Johansson, R., and Kosma, V.M. (2005). Expression of CD 44 s, CD 44 v 3 and CD 44 v 6 in benign and malignant breast lesions: correlation and colocalization with hyaluronan. Histopathology *47*, 420–428.
17. Bànkfalvi, A., Terpe, H.J., Breukelmann, D., Bier, B., Rempe, D., Pschadka, G., Krech, R., Lellè, R.J., and Boecker, W. (1999). Immunophenotypic and prognostic analysis of E-cadherin and beta-catenin expression during breast carcinogenesis and tumour progression: a comparative study with CD44. Histopathology *34*, 25–34.
18. Oda, Y., Aishima, S., Morimatsu, K., Hayashi, A., Shindo, K., Fujino, M., Mizuuchi, Y., Hattori, M., Tanaka, M., and Oda, Y. (2013). Differential ezrin and phosphorylated ezrin expression profiles between pancreatic intraepithelial neoplasia, intraductal papillary mucinous neoplasm, and invasive ductal carcinoma of the pancreas. Hum. Pathol. *44*, 1487–1498.
19. Kalantari, E., Asgari, M., Nikpanah, S., Salarieh, N., Asadi Lari, M.H., and Madjd, Z. (2017). Co-expression of putative cancer stem cell markers CD44 and CD133 in prostate carcinomas. Pathol. Oncol. Res. *23*, 793–802.
20. Morrison, H., Sherman, L.S., Legg, J., Banine, F., Isacke, C., Haipek, C.A., Gutmann, D.H., Ponta, H., and Herrlich, P. (2001). The NF2 tumor suppressor gene product, merlin, mediates contact inhibition of growth through interactions with CD44. Genes Dev. *15*, 968–980.
21. Natsuga, K., Watanabe, M., Nishie, W., and Shimizu, H. (2019). Life before and beyond blistering: The role of collagen XVII in epidermal physiology. Exp. Dermatol. *28*, 1135–1141.
22. Owens, D.W., McLean, G.W., Wyke, A.W., Paraskeva, C., Parkinson, E.K., Frame, M.C., and Brunton, V.G. (2000). The catalytic activity of the Src family kinases is required to disrupt cadherin-dependent cell-cell contacts. Mol. Biol. Cell *11*, 51–64.
23. Huber, B.E., and Cordingley, M.G. (1988). Expression and phenotypic alterations caused by an inducible transforming ras oncogene introduced into rat liver epithelial cells. Oncogene *3*, 245–256.
24. Lindsay, J., Jiao, X., Sakamaki, T., Casimiro, M.C., Shirley, L.A., Tran, T.H., Ju, X., Liu, M., Li, Z., Wang, C., et al. (2008). ErbB2 induces Notch1 activity and function in breast cancer cells. Clin. Transl. Sci. *1*, 107–115.
25. Marinari, E., Mehonic, A., Curran, S., Gale, J., Duke, T., and Baum, B. (2012). Live-cell delamination counterbalances epithelial growth to limit tissue overcrowding. Nature *484*, 542–545.
26. Eisenhoffer, G.T., Loftus, P.D., Yoshigi, M., Otsuna, H., Chien, C.B., Morcos, P.A., and Rosenblatt, J. (2012). Crowding induces live cell extrusion to maintain homeostatic cell numbers in epithelia. Nature *484*, 546–549.
27. Makohon-Moore, A., and Iacobuzio-Donahue, C.A. (2016). Pancreatic cancer biology and genetics from an evolutionary perspective. Nat. Rev. Cancer *16*, 553–565.
28. Brown, C.W., Amante, J.J., Goel, H.L., and Mercurio, A.M. (2017). The $\alpha 6\beta 4$ integrin promotes resistance to ferroptosis. J. Cell Biol. *216*, 4287–4297.
29. Dixon, S.J., Lemberg, K.M., Lamprecht, M.R., Skouta, R., Zaitsev, E.M., Gleason, C.E., Patel, D.N., Bauer, A.J., Cantley, A.M., Yang, W.S., et al. (2012). Ferroptosis: an iron-dependent form of nonapoptotic cell death. Cell *149*, 1060–1072.
30. Kleppner, S.R., and Tobin, A.J. (2002). GABA. In Encyclopedia of the Human Brain, First Edition, V.S. Ramachandran, ed. (Elsevier), pp. 353–367.
31. Chouchani, E.T., Pell, V.R., Gaude, E., Aksentijević, D., Sundier, S.Y., Robb, E.L., Logan, A., Nadtochiy, S.M., Ord, E.N.J., Smith, A.C., et al. (2014). Ischaemic accumulation of succinate controls reperfusion injury through mitochondrial ROS. Nature *515*, 431–435.
32. Mills, E.L., Kelly, B., Logan, A., Costa, A.S.H., Varma, M., Bryant, C.E., Tourlomousis, P., Däbritz, J.H.M., Gottlieb, E., Latorre, I., et al. (2016). Succinate dehydrogenase supports metabolic repurposing of mitochondria to drive inflammatory macrophages. Cell *167*, 457–470.e13.
33. Hofmann, M., Rudy, W., Günthert, U., Zimmer, S.G., Zawadzki, V., Zöller, M., Lichtner, R.B., Herrlich, P., and Ponta, H. (1993). A link between ras and metastatic behavior of tumor cells: ras induces CD44 promoter activity and leads to low-level expression of metastasis-specific variants of CD44 in CREF cells. Cancer Res. *53*, 1516–1521.
34. Jamal, H.H., Cano-Gauci, D.F., Buick, R.N., and Filmus, J. (1994). Activated ras and src induce CD44 overexpression in rat intestinal epithelial cells. Oncogene *9*, 417–423.
35. Zhao, B., Wei, X., Li, W., Udan, R.S., Yang, Q., Kim, J., Xie, J., Ikenoue, T., Yu, J., Li, L., et al. (2007). Inactivation of YAP oncoprotein by the Hippo pathway is involved in cell contact inhibition and tissue growth control. Genes Dev. *21*, 2747–2761.
36. Levayer, R., Dupont, C., and Moreno, E. (2016). Tissue crowding induces caspase-dependent competition for space. Curr. Biol. *26*, 670–677.
37. Moreno, E., Valon, L., Levillayer, F., and Levayer, R. (2019). Competition for space induces cell elimination through compaction-driven ERK downregulation. Curr. Biol. *29*, 23–34.e8.
38. Hogan, C., Dupré-Crochet, S., Norman, M., Kajita, M., Zimmermann, C., Pelling, A.E., Piddini, E., Baena-López, L.A., Vincent, J.P., Itoh, Y., et al. (2009). Characterization of the interface between normal and transformed epithelial cells. Nat. Cell Biol. *11*, 460–467.
39. Kon, S., Ishibashi, K., Katoh, H., Kitamoto, S., Shirai, T., Tanaka, S., Kajita, M., Ishikawa, S., Yamauchi, H., Yako, Y., et al. (2017). Cell competition with normal epithelial cells promotes apical extrusion of transformed cells through metabolic changes. Nat. Cell Biol. *19*, 530–541.
40. Sasaki, A., Nagatake, T., Egami, R., Gu, G., Takigawa, I., Ikeda, W., Nakatani, T., Kunisawa, J., and Fujita, Y. (2018). Obesity suppresses cell-competition-mediated apical elimination of RasV12-transformed cells from epithelial tissues. Cell Rep. *23*, 974–982.
41. Kajita, M., Sugimura, K., Ohoka, A., Burden, J., Suganuma, H., Ikegawa, M., Shimada, T., Kitamura, T., Shindoh, M., Ishikawa, S., et al. (2014). Filamin acts as a key regulator in epithelial defence against transformed cells. Nat. Commun. *5*, 4428.
42. Porazinski, S., de Navascués, J., Yako, Y., Hill, W., Jones, M.R., Maddison, R., Fujita, Y., and Hogan, C. (2016). EphA2 drives the segregation of Ras-transformed epithelial cells from normal neighbors. Curr. Biol. *26*, 3220–3229.
43. Ishimoto, T., Nagano, O., Yae, T., Tamada, M., Motohara, T., Oshima, H., Oshima, M., Ikeda, T., Asaba, R., Yagi, H., et al. (2011). CD44 variant regulates redox status in cancer cells by stabilizing the xCT subunit of system xc(-) and thereby promotes tumor growth. Cancer Cell *19*, 387–400.
44. Waters, A.M., and Der, C.J. (2018). KRAS: the critical driver and therapeutic target for pancreatic cancer. Cold Spring Harb. Perspect. Med. *8*, a031435.
45. Vincent, A., Herman, J., Schulick, R., Hruban, R.H., and Goggins, M. (2011). Pancreatic cancer. Lancet *378*, 607–620.

46. Kleeff, J., Korc, M., Apte, M., La Vecchia, C., Johnson, C.D., Biankin, A.V., Neale, R.E., Tempero, M., Tuveson, D.A., Hruban, R.H., and Neoptolemos, J.P. (2016). Pancreatic cancer. Nat. Rev. Dis. Primers *2*, 16022.

47. Rhim, A.D., Mirek, E.T., Aiello, N.M., Maitra, A., Bailey, J.M., McAllister, F., Reichert, M., Beatty, G.L., Rustgi, A.K., Vonderheide, R.H., et al. (2012). EMT and dissemination precede pancreatic tumor formation. Cell *148*, 349–361.

48. Maruyama, T., Dougan, S.K., Truttmann, M.C., Bilate, A.M., Ingram, J.R., and Ploegh, H.L. (2016). Corrigendum: increasing the efficiency of precise genome editing with CRISPR-Cas9 by inhibition of nonhomologous end joining. Nat. Biotechnol. *34*, 210.

49. Ohoka, A., Kajita, M., Ikenouchi, J., Yako, Y., Kitamoto, S., Kon, S., Ikegawa, M., Shimada, T., Ishikawa, S., and Fujita, Y. (2015). EPLIN is a crucial regulator for extrusion of RasV12-transformed cells. J. Cell Sci. *128*, 781–789.

50. Hsu, P.D., Scott, D.A., Weinstein, J.A., Ran, F.A., Konermann, S., Agarwala, V., Li, Y., Fine, E.J., Wu, X., Shalem, O., et al. (2013). DNA targeting specificity of RNA-guided Cas9 nucleases. Nat. Biotechnol. *31*, 827–832.

51. Kajita, M., Hogan, C., Harris, A.R., Dupre-Crochet, S., Itasaki, N., Kawakami, K., Charras, G., Tada, M., and Fujita, Y. (2010). Interaction with surrounding normal epithelial cells influences signalling pathways and behaviour of Src-transformed cells. J. Cell Sci. *123*, 171–180.

52. Hogan, C., Serpente, N., Cogram, P., Hosking, C.R., Bialucha, C.U., Feller, S.M., Braga, V.M., Birchmeier, W., and Fujita, Y. (2004). Rap1 regulates the formation of E-cadherin-based cell-cell contacts. Mol. Cell. Biol. *24*, 6690–6700.

53. Marks, J.D., and Bradbury, A. (2004). Selection of human antibodies from phage display libraries. Methods Mol. Biol. *248*, 161–176.

54. Naruse, K., Yamada, T., Sai, X.R., Hamaguchi, M., and Sokabe, M. (1998). Pp125FAK is required for stretch dependent morphological response of endothelial cells. Oncogene *17*, 455–463.

55. Satoh, K., Yachida, S., Sugimoto, M., Oshima, M., Nakagawa, T., Akamoto, S., Tabata, S., Saitoh, K., Kato, K., Sato, S., et al. (2017). Global metabolic reprogramming of colorectal cancer occurs at adenoma stage and is induced by MYC. Proc. Natl. Acad. Sci. USA *114*, E7697–E7706.

56. Soga, T., Baran, R., Suematsu, M., Ueno, Y., Ikeda, S., Sakurakawa, T., Kakazu, Y., Ishikawa, T., Robert, M., Nishioka, T., and Tomita, M. (2006). Differential metabolomics reveals ophthalmic acid as an oxidative stress biomarker indicating hepatic glutathione consumption. J. Biol. Chem. *281*, 16768–16776.

57. Soga, T., Igarashi, K., Ito, C., Mizobuchi, K., Zimmermann, H.P., and Tomita, M. (2009). Metabolomic profiling of anionic metabolites by capillary electrophoresis mass spectrometry. Anal. Chem. *81*, 6165–6174.

58. Yang, M., Soga, T., and Pollard, P.J. (2013). Oncometabolites: linking altered metabolism with cancer. J. Clin. Invest. *123*, 3652–3658.

59. Isokawa, M., Funatsu, T., and Tsunoda, M. (2013). Fast and simultaneous analysis of biothiols by high-performance liquid chromatography with fluorescence detection under hydrophilic interaction chromatography conditions. Analyst (Lond.) *138*, 3802–3808.

Please cite this article in press as: Kozawa et al., The CD44/COL17A1 pathway promotes the formation of multilayered, transformed epithelia, Current Biology (2021), https://doi.org/10.1016/j.cub.2021.04.078

STAR★METHODS

KEY RESOURCES TABLE

REAGENT or RESOURCE	SOURCE	IDENTIFIER
Antibodies		
mouse anti-β-actin antibody	Millipore	Cat#MAB1501R clone C4; RRID: AB_2223041
mouse anti-GAPDH antibody	Millipore	Cat#MAB374; RRID: AB_2107445
mouse anti-GAPDH antibody	Santa Cruz Biotechnology	Cat#sc32233; RRID: AB_627679
mouse anti-γ-tubulin antibody	Abcam	Cat#ab11316; RRID: AB_297920
rabbit anti-COL17A1 antibody	Abcam	ab186415
rabbit anti-phospho p44/42 MAPK (Erk1/2) antibody	Cell Signaling Technology	Cat#4370; RRID: AB_2315112
rabbit anti-p44/42 MAPK (Erk1/2) antibody	Cell Signaling Technology	Cat#4695; RRID: AB_390779
rabbit anti-Akt antibody	Cell Signaling Technology	Cat#9272; RRID: AB_329827
rabbit anti-phospho-Akt (Ser473) antibody	Cell Signaling Technology	Cat#9271; RRID: AB_329825
mouse anti-GFP antibody	Roche	Cat#11814460001; RRID: AB_390913
rat anti-HA antibody	Roche	Cat#11867423001; RRID: AB_390918
rat anti-E-cadherin antibody	Life Technologies	Cat#13-1900; RRID: AB_2533005
rabbit anti-pericentrin antibody	BioLegend	Cat#923701; RRID: AB_2565440
rabbit anti-ZO-1 antibody	ZYMED	Cat#61-7300; RRID: AB_2533938
rat anti-CD44 antibody	Invitrogen	Cat#14-0441-82; RRID: AB_467246
rat anti-CD44 antibody	TONBO	Cat#70-0441; RRID: AB_2621494
rabbit anti-CD44 antibody	Bethyl Laboratories	Cat#A303-872A; RRID: AB_2620223
mouse anti-FLAG antibody	Sigma-Aldrich	Cat#F3165; RRID: AB_259529
human anti-COL17A1 (1C10) antibody	This paper	N/A
human anti-COL17A1 (20C5) antibody	This paper	N/A
Alexa Fluor-568-conjugated phalloidin	Life Technologies	A12380
Alexa Fluor-647-conjugated phalloidin	Life Technologies	A22287
Chemicals, peptides, and recombinant proteins		
U0126	Promega	V1121
Cycloheximide	Sigma-Aldrich	01810
Ferrostatin (Fer)-1	Sigma-Aldrich	SML0583
CCCP	Sigma-Aldrich	C2759
Rotenone	Sigma-Aldrich	R8875
LY294002	Calbiochem	440202
Z-VAD-FMK	Calbiochem	219007
Trolox	Cayman Chemical	10011659
G418 (Geneticin)	GIBCO	10131027
puromycin	Sigma-Aldrich	P8833
doxycycline	Sigma-Aldrich	D3447
tetracycline	Sigma-Aldrich	T7660
Trizol	Thermo Fisher Scientific	15596026
Critical commercial assays		
SiR-actin Kit	SPIROCHROME	CY-SC001
Hoechst 33342	Life Technologies	H3570
Type I collagen	Nitta Gelatin	N/A
MycoAlart	Lonza	LT07-118
Nucleofector 2b Kit L	Lonza	VACA-1005
Lipofectamine 2000	Life Technologies	11668019

(*Continued on next page*)

Please cite this article in press as: Kozawa et al., The CD44/COL17A1 pathway promotes the formation of multilayered, transformed epithelia, Current Biology (2021), https://doi.org/10.1016/j.cub.2021.04.078

Continued

REAGENT or RESOURCE	SOURCE	IDENTIFIER
RNeasy Mini Kit	QIAGEN	74104
QuantiTect Reverse Transcription Kit	QIAGEN	205311
GeneAce SYBR qPCR Mix	NIPPON GENE	319-07683
TMRM	Thermo Fisher Scientific	T668
MitoSOX	Thermo Fisher Scientific	M36008
2-NBDG	Cayman Chemical	11046
SYTOX Orange	Molecular Probes	S11368
C11-BODIPY	Molecular Probes	D3861
Click-iT EdU Cell Proliferation Kit	Invitrogen	C10340
STB-100 cell stretcher system	Strex	STB-100
Deposited data		
Metabolome analysis data	This paper	https://molonc.researcherinfo.net/metabolome1.pdf.
Experimental models: cell lines		
MDCK	Dr. W. Birchmeier	N/A
MCF10A	Dr. K Semba	N/A
HPDE	Cell Biologics Inc	H-6037
Experimental models: organisms/strains		
KPC mice	Dr. A. Enomoto	N/A
Mice, wildtype	Dr. A. Enomoto	N/A
Oligonucleotides		
CD44-shRNA-1 forward: 5′-ATCTGCTCCACC TGAAGAGGATTGTACTCGAGAACAA TCCTCTTCAGGTGGAGCTTTTTC-3′	This paper	N/A
CD44-shRNA-1 reverse: 5′-CGAGAAAAAGCTC CACCTGAAGAGGATTGTTCTCGAGTA CAATCCTCTTCAGGTGGAGCA-3′	This paper	N/A
CD44-shRNA-2 forward: 5′-ATCTGACCACGAC TCATCGGTTCACACTCGAGAGTGA ACCGATGAGTCGTGGTCTTTTTC-3′	This paper	N/A
CD44-shRNA-2 reverse: 5′-TCGAGAAAAAGA CCACGACTCATCGGTTCACTCTCGA GTGTGAACCGATGAGTCGTGGTCA-3′	This paper	N/A
COL17A1-sgRNA1 sequence: 5′-CCCGCCATGGAACATACGA-3′	This paper	N/A
COL17A1-sgRNA2 sequence: 5′-TCCTCGGAAGGAGTTCGGT-3′	This paper	N/A
Primer, COL17A1-sgRNA1 forward: 5′-TTCAAGCCAGTCCGAAGTGC-3′	This paper	N/A
Primer, COL17A1-sgRNA1 reverse: 5′-GTCTCTCCTTCTCCCTTTGTCC-3′	This paper	N/A
Primer, COL17A1-sgRNA2 forward: 5′-CCACAACTGTGTCCAGCAGG-3′	This paper	N/A
Primer, COL17A1-sgRNA1 reverse: 5′-GCCTGAGCCTTGTGTGAATAAC-3′	This paper	N/A
Primer, COL17A1 forward: 5′-ACTACTCAGAGCTGGCAAGC-3′	This paper	N/A
Primer, COL17A1 reverse: 5′-CAGCCACAATGTCCTCCGTAG-3′	This paper	N/A
Primer, ABAT forward: 5′-AGCAAGAAGAAGCCCGCTGC-3′	This paper	N/A

(*Continued on next page*)

Please cite this article in press as: Kozawa et al., The CD44/COL17A1 pathway promotes the formation of multilayered, transformed epithelia, Current Biology (2021), https://doi.org/10.1016/j.cub.2021.04.078

Continued

REAGENT or RESOURCE	SOURCE	IDENTIFIER
Primer, ABAT reverse: 5′-CTCAGACTGGATGGGCTCC-3′	This paper	N/A
Primer, ALDH5A1 forward: 5′-GGCGTGGCTGCAGTCATCAC-3′	This paper	N/A
Primer, ALDH5A1 reverse: 5′-GACAGTACAGCCGGCTGCCA-3′	This paper	N/A
Primer, GAD2 forward: 5′-AAGCGGAGGTCAACTATGCG-3′	This paper	N/A
Primer, GAD2 reverse: 5′-CATCACAGGCTGGCAGCAG-3′	This paper	N/A
Primer, β-actin forward: 5′-GGCACCCAGCACAATGAAG-3′	This paper	N/A
Primer, β-actin reverse: 5′-ACAGTGAGGCCAGGATGGAG-3′	This paper	N/A
Recombinant DNA		
pCDH-EF1-Hygro-sgRNA vector	Maruyama et al.[48]	N/A
pCDH-EF1-COL17A1 sgRNA	This paper	N/A
Software and algorithms		
Metamorph	Molecular Devices	https://www.moleculardevices.co.jp/systems/metamorph-microscopy-automation-and-image-analysis-software
ImageJ	NIH Image	https://imagej.nih.gov/ij/download.html
GraphPad Prism 7	GraphPad Software	https://www.mdf-soft.com/products/graphpad_prism8.html

RESOURCE AVAILABILITY

Lead contact

Further information and requests for resources and reagents should be directed to and will be fulfilled by the Lead Contact, Yasuyuki Fujita (fujita@monc.med.kyoto-u.ac.jp).

Materials availability

This study did not generate new unique reagents. Plasmids or cell lines generated in this study will be made available on request, but we may require a payment and/or a completed Materials Transfer Agreement if there is potential for commercial application.

Data and code availability

The metabolome analysis data generated during this study are available at https://molonc.researcherinfo.net/metabolome1.pdf. All the other data associated with the paper is available upon request.

EXPERIMENTAL MODEL AND SUBJECT DETAILS

MDCK, MCF10A, and HPDE cells were used in this study. The parental MDCK cells were a gift from Dr. Walter Birchmeier. Mycoplasma contamination is regularly tested for all cell lines using a commercially available kit (MycoAlert, Lonza). MCF10A Tet-on Ad ErbB2V659E cells are a gift from Dr. Kentaro Semba and were cultured in DMEM/F12 (Life Technologies) containing 5% horse serum (Life technology), 20 ng ml^{-1} EGF (BD bioscience), 0.5 μg ml^{-1} Hydrocortisone (Sigma-Aldrich), 100 ng ml^{-1} Cholera Toxin (List Biological Laboratories), 10 μg ml^{-1} Insulin (Sigma-Aldrich), 0.5 μg ml^{-1} G418 (Calbiochem), and 1% penicillin/streptomycin (Life Technologies). HPDE cells were from Cell Biologics, Inc. and cultured in DMEM/F12 (Life Technologies) containing 2 mg ml^{-1} bovine serum albumin (Wako), Insulin (10 μg ml^{-1})-Tranferrin (5.5 μg ml^{-1})-Selenium (6.7 ng ml^{-1}) (ITS) (Life Technologies), 1 × Antibiotic-Antimycotic (Life Technologies), 5 mM Nicotinamide, 50 ng ml^{-1} recombinant human EGF, and 25 ng ml^{-1} recombinant human FGF10 at 37°C in a 3% O_2 incubator.

METHOD DETAILS

Antibodies, Plasmids, and Materials

The following primary antibodies were used in this study: mouse anti-β-actin (MAB1501) and mouse anti-GAPDH (MAB374) antibodies from Merck Millipore, mouse anti-GAPDH (sc32233) antibody from Santa Cruz Biotechnology, mouse anti-γ-tubulin

(ab11316) and rabbit anti-COL17A1 (ab186415) antibodies from Abcam, rabbit anti-phospho p44/42 MAPK (Erk1/2) (#4370), rabbit anti-p44/42 MAPK (Erk1/2) (#4695), rabbit anti-Akt (#9272), and rabbit anti-phospho-Akt (Ser473) (#9271) antibodies from Cell Signaling Technology, mouse anti-GFP (11814460001) and rat anti-HA (11867423001) antibodies from Roche, rat anti-E-cadherin (13-1900) antibody from Life Technologies, rabbit anti-pericentrin (923701) antibody from BioLegend, rabbit anti-ZO-1 (61-7300) antibody from ZYMED, rat anti-CD44 antibody from Invitrogen (14-0441-82) or TONBO (70-0441), rabbit anti-CD44 (A303-872A) antibody from Bethyl Laboratories, mouse anti-FLAG (F3165) antibody from Sigma-Aldrich. Mouse anti-GAPDH (MAB374) or mouse anti-GAPDH (sc32233) antibody was used for Figures S1E and S5I or Figures 1B, 2C, 5F, S1C, and S2A, respectively. Rat anti-CD44 (14-0441-82) or rat anti-CD44 (70-0441) antibody was used for immunofluorescence or immunohistochemistry for Figures 5B, S5B, S5K, and S5M or Figures 5A, S5A, and S5C, respectively. Rabbit anti-CD44 antibody was used for western blotting. Mouse anti-gp135 antibody was kindly provided by Dr. George Ojakian. Alexa Fluor-568- and −647-conjugated phalloidin (Life Technologies) were used at 1.0 U ml^{-1}. Alexa Fluor-488-, −568-, and −647-conjugated secondary antibodies were from Life Technologies. Hoechst 33342 (Life Technologies) was used at a dilution of 1:5,000 for immunofluorescence. U0126 (10 μM) was from Promega. Cycloheximide (50 μM), Ferrostatin (Fer)-1 (20 μM), CCCP (5 μM), and Rotenone (5 μM) were from Sigma-Aldrich. LY294002 (50 μM) and Z-VAD-FMK (50 μM) were from Calbiochem. Trolox (1 mM) was from Cayman Chemical. The SiR-Actin Kit (far-red silicon rhodamine (SiR)-Actin fluorescence probe) was obtained from SPIROCHROME for live imaging of F-actin and was used according to the manufacturer's instructions.

Establishment of Cell Lines

MDCK cells stably expressing GFP (MDCK-pTR GFP), GFP-H-RasV12 (MDCK-pTR GFP-H-RasV12), GFP-K-RasV12 (MDCK-pTR GFP-K-RasV12) or GFP-cSrcY527F (MDCK-pTR GFP-cSrcY527F) in a tetracycline-inducible manner were established and cultured as previously described[38,49]. To establish CRISPR/Cas9-mediated COL17A1-knockout MDCK cells, guide sequences of COL17A1 single-guide RNA (sgRNA) targeting Canis COL17A1 were designed on exon 4 or 5 as described previously[50]. COL17A1-sgRNA sequence (COL17A1-sgRNA1: 5′-CCCGCCATGGAACATACGA-3′ or COL17A1-sgRNA2: 5′-TCCTCGGAAGGAGTTCGGT-3′) was introduced into the pCDH-EF1-Hygro-sgRNA vector. First, MDCK cells were infected with lentivirus carrying pCW-Cas9 as described[48] and were cultured in the 500 ng ml^{-1} puromycin-containing medium. The tetracycline-inducible MDCK-Cas9 cells were transfected with pCDH-EF1-COL17A1-sgRNA1 or 2 by nucleofection, followed by selection in the medium containing 200 μg ml^{-1} of hygromycin, and subjected to limiting dilution. Indels on the COL17A1 exons in each monoclone were analyzed by direct sequencing using the following primers (for COL17A1-sgRNA1: 5′-TTCAAGCCAGTCCGAAGTGC-3′ and 5′-GTCTCTCCTTCTCCCTTTGTCC-3′ or for COL17A1-sgRNA2: 5′-CCACAACTGTGTCCAGCAGG-3′ and 5′-GCCTGAGCCTTGTGTGAATAAC-3′). To generate MDCK-pTRE3G GFP-RasV12 COL17A1-knockout or MDCK-pTRE3G Myc-RasV12 COL17A1-knockout cells, the complementary DNA of GFP-H-RasV12 or Myc-H-RasV12 was cloned into BamHI/EcoRI sites of pPB-TRE3G-MCS-CEH-rtTA3-IP[39]. pPB-TRE3G GFP-H-RasV12 or pPB-TRE3G Myc-H-RasV12 was introduced into the COL17A1-depleted cells by nucleofection and antibiotic selection (blasticidin, 5 μg ml^{-1}). For COL17A1-knockout RasV12 cells, MDCK-pTRE3G Myc-RasV12 COL17A1-knockout cells were used in Figures 4A, S4A, and S4C, while MDCK-pTRE3G GFP-RasV12 COL17A1-knockout cells were used in the other experiments. MDCK-pTR GFP-H-RasV12 cells stably expressing CD44-short hairpin RNA (shRNA) were established as follows: CD44-shRNA oligonucleotides (CD44-shRNA-1: 5′-GATCTGCTCCACCTGAAGAGGATTGTACTCGAGAACAATCCTCTTCAGGTGGAGCTTTTTC-3′ and 5′-TCGAGAAAAAGCTCCACCTGAAGAGGATTGTTCTCGAGTACAATCCTCTTCAGGTGGAGCA-3′ or CD44-shRNA-2: 5′-GATCTGACCACGACTCATCGGTTCACACTCGAGAGTGAACCGATGAGTCGTGGTCTTTTTC-3′ and 5′-TCGAGAAAAAGACCACGACTCATCGGTTCACTCTCGAGTGTGAACCGATGAGTCGTGGTCA-3′) were cloned into the BglII/XhoI sites of pSUPER.neo (Oligoengine). MDCK-pTR GFP-H-RasV12 cells were transfected with pSUPER.neo CD44-shRNA using Lipofectamine 2000, followed by selection in the medium containing 5 μg ml^{-1} blasticidin, 400 μg ml^{-1} Zeocin, and 800 μg ml^{-1} G418. To generate HPDE-pTRE3G GFP-K-RasV12 cells, the complementary DNA of GFP-K-RasV12 was cloned into BamHI/EcoRI sites of pPB-TRE3G-MCS-CEH-rtTA3-IP. pPB-TRE3G GFP-K-RasV12 was introduced into HPDE cells by nucleofection and antibiotic selection (blasticidin, 10 μg ml^{-1}).

Immunofluorescence and Western Blotting

For immunofluorescence at low, middle, or high cell density, 1.0×10^4, 6.5×10^5, or 1.0×10^6 cells were plated respectively onto collagen gel-coated coverslips in a 12-well dish (Falcon). For most of experiments for immunofluorescence, 6.5×10^5 cells were plated if not indicated. After incubation for 24ch, cells were fixed with 4% paraformaldehyde (PFA) in phosphate-buffered saline (PBS) and permeabilized as previously described[51]. Type-I collagen (Cellmatrix Type I-A) was obtained from Nitta Gelatin and was neutralized on ice to a final concentration of 2cmgcml^{-1} according to the manufacturer's instructions. All primary antibodies were used at 1:100, except for human anti-COL17A1 (1C10 or 20C5) antibody at 1:1,000. All secondary antibodies were used at 1:200. Immunofluorescence images were analyzed with the Olympus FV1000 or FV1200, or ZEISS LSM700 system and Olympus FV10-ASW or ZEISS ZEN software. Images were quantified with the MetaMorph software (Molecular Devices) and ImageJ. For transient expression of GFP, GFP-RasV12, GFP-Rap1V12, GFP-cSrcY527F, or HA-ErbB2V659E, normal MDCK cells were transfected with pcDNA4/TO-EGFP, pcDNA4/TO-EGFP-RasV12, pCS2-EGFP-Rap1V12, pcDNA4/TO-EGFP-cSrcY527F, or pB-EF1-ErbB2V659E-HA using Lipofectamine 2000 as previously described[41]. For quantification of multilayered structures of MDCK cells, 15 xz sections of immunofluorescence images of MDCK cells from 5 randomly selected fields (212 × 212 μm) were analyzed for each condition. From the xz section of immunofluorescence images, the horizontal length of the 1st, 2nd, and more than 3rd layer

Please cite this article in press as: Kozawa et al., The CD44/COL17A1 pathway promotes the formation of multilayered, transformed epithelia, Current Biology (2021), https://doi.org/10.1016/j.cub.2021.04.078

was quantified. The ratio of multilayered regions was calculated as a relative ratio to the total length. For measuring spindle angles during mitosis, cells were plated on a coverslip and grown to confluence for 24 h. Pericentrin and γ-tubulin were used to indicate spindle pole positions. The spindle angle between the axis of spindle poles and the surface of coverslip was calculated with ImageJ. Fifty mitotic spindles were scored in each experiment. To monitor the mitochondrial membrane potential or superoxide production, cells were cultured for 24 h after seeding and then loaded with 50 nM TMRM (Thermo Fisher Scientific) or 5 μM MitoSOX (Thermo Fisher Scientific) respectively for 30 min, followed by microscopic observation as previously described[39]. The 2-NBDG (Cayman Chemical) uptake was examined by incubating cells in glucose-free DMEM for 2 h followed by incubation with 100 μM 2-NBDG for 30 min as previously described[39]. For quantification of the frequency of cell death during crowding cell extrusion, cells were incubated for 12 h after plating and stained with SYTOX Orange and SiR-Actin probe. After culturing for 12 h, SYTOX-positive or -negative extruded cells that detached from the basal layer were analyzed in 5 randomly selected fields (317 × 317 μm) with the Olympus FV1000 or FV1200 system. For quantification of the frequency of cell death in multilayered structures, cells were incubated for 36 h and stained with SYTOX Orange (Molecular Probes) to label dead cells according to the manufacturer's instructions. After 12 h, ten randomly selected fields (2,048 × 2,048 pixels) at the upper layers were photographed (x60) under a phase-contrast microscope. To measure lipid peroxidation, MDCK cells were cultured for 24 h after seeding and then fluorescently labeled with C11-BODIPY (Molecular Probes) according to manufacturer's instructions. The level of lipid peroxidation was determined by quantitating the ratio of fluorescence intensities (oxidized form at 488-nm channel to non-oxidized form at 590-nm channel). For EdU incorporation assay, EdU incorporation into newly synthesized DNA was measured using a Click-iT EdU Cell Proliferation Kit (Invitrogen) according to manufacturer's instructions. For immunofluorescence of incorporated EdU, cells were cultured for 48 h, followed by treatment with 50 μM EdU for 1 h and fixation with 4% PFA. The fixed samples were processed for the EdU Click-iT reaction, and additional immunofluorescence was carried out with anti-E-cadherin antibody and Hoechst. For quantification of EdU incorporation ratio in multilayered structures of MDCK cells, 15 xz sections of immunofluorescence images from 5 randomly selected fields (212 × 212 μm) were analyzed for each cell type in each experiment by the Olympus FV1200. Western blotting was performed as previously described[52]. Primary antibodies were used at 1:1,000. Western blotting data were analyzed using ImageQuant LAS4010 (GE healthcare) or Chem-iDoc Touch Imaging System (Bio-Rad Laboratories).

Phage Antibody Display Screening

Phage antibody libraries containing FLAG-tagged single chain Fvs (scFvs) were generated at the KAN Research Institute, Inc. For pre-blocking of cells and preclear/selection steps, 2% skim milk/DMEM was used. For the preclear step, 1.0×10^7 MDCK cells were cultured alone in a 10-cm dish. Cells were then incubated with phage antibodies at 4°C for 1 h on a shaker. The preclear step was repeated twice at every round, and the unbound phage antibodies were used for the selection step. For the selection step, 9.1×10^6 MDCK cells were co-cultured with 9.0×10^5 MDCK-pTR GFP-RasV12 cells in a 10-cm dish. The mixture of cells was first incubated at 37°C for 8 h until a monolayer was formed, and the culture medium was exchanged for a new medium containing 2 μg ml^{-1} tetracycline to induce expression of GFP-RasV12, followed by incubation for 16 h. Cells were then incubated with the unbound phage antibodies at 4°C for 2 h on a shaker. The unbound phage antibodies were removed, and the cells with bound phage antibodies were washed 5 times with 0.05% Tween 20/PBS. Then, 1.0 mL of 100 mM triethylamine was added to the cell pellets to elute bound phage antibodies, which was neutralized immediately by adding 0.5 mL of 1.0 M Tris-HCl, pH 8.0. The eluant was added to exponentially growing *E. coli* TG1 (OD_{600} ~0.5) and incubated without shaking at 37°C for 30 min. The infected *E. coli* were plated on LB/ampicillin/glucose plates and incubated at 30°C overnight. The *E. coli* were collected from the plates, amplified and purified with polyethylene glycol according to the reported protocol[53]. The purified phage antibodies were used for the next round. After three rounds, individual colonies of *E. coli* infected with phage antibodies were picked up into 96-well microtiter plate wells containing 2X YT/ampicillin/glucose and grown with shaking at 37°C (OD_{600} ~0.5). IPTG (isopropyl β-D-thiogalactopyranoside) was added to the *E. coli* culture to a final concentration of 1 mM and incubated at 30°C overnight to induce FLAG-tagged scFvs. For immunofluorescence screening, 4.0×10^4 MDCK cells were mixed with 1.3×10^3 MDCK-pTR GFP-H-RasV12 cells and seeded into a 96 well of Half Area High Content Imaging Film Bottom Microplate (Corning), followed by the induction of GFP-RasV12 expression as described above. Cells were then incubated with FLAG-tagged scFvs for 1 h, fixed with 1% PFA for 10 min, incubated with anti-FLAG antibody for 1 h, and then stained with Alexa-568-conjugated anti-mouse IgG and Hoechst for 1 h. The images of cells were captured by confocal inverted microscope Eclipse Ti (Nikon) using the Revolution XD system (Andor), followed by the analysis of scFv staining with the MetaMorph Imaging software.

Immunoprecipitation and Mass Spectrometry

For immunoprecipitation, the indicated 1.0×10^7 cells were seeded in a 10-cm dish and cultured for 24 h. Cells were then washed with ice-cold PBS and lysed for 30 min in M-PER Mammalian Protein Extraction Reagent (Thermo Fisher Scientific) containing cOmplete Protease Inhibitor Cocktail (Roche). After centrifugation of the cell lysates at 15,000cg for 5cmin, the supernatants were subjected to immunoprecipitation for 1 h with Protein A/G Magnetic Beads (Pierce) conjugated with 5 μg of clone 1C10 or clone 20C5 antibody. Immunoprecipitated proteins were subjected to SDS-PAGE, followed by silver staining (2D-Silver Stain Reagent II kit from COSMO BIO) according to the manufacturer's instructions. Protein bands were excised from the gel, and the protein was identified by LC/MS/MS analysis. Briefly, protein bands were cut into pieces and digested in-gel by Lys-C (Wako) and subsequently by modified trypsin Porcine (Promega) after reductive S-alkylation with dithiothreitol and iodoacetamide. After incubation at 37°C overnight, tryptic peptides were purified by tip column packed with Empore C18 and dried. Peptides were

Please cite this article in press as: Kozawa et al., The CD44/COL17A1 pathway promotes the formation of multilayered, transformed epithelia, Current Biology (2021), https://doi.org/10.1016/j.cub.2021.04.078

dissolved with 0.1% TFA-5% acetonitrile and analyzed by Q Exactive HF mass spectrometry (Thermo Fisher Scientific). The raw data were analyzed using Proteome Discoverer Ver 2.2 (Thermo Fisher Scientific), and proteins were identified against canis familiaris database (UniProt) on SEQUEST.

Compression or Stretching Assay

Mechanical compaction and stretching experiments were performed using the STB-100 cell stretcher system (Strex) for cells cultured on a flexible silicone membrane PDMS (polydimethylpolysiloxane) (20 mm x 20 mm)[54]. For compression assay, before cell seeding, silicone membranes were stretched (20 mm x 25 mm) and coated with 5 μg ml^{-1} fibronectin (Sigma-Aldrich) at 37°C for 1 h. Then, 1.0 × 10^6 RasV12-transformed MDCK cells were plated onto the stretched silicone membrane, grown to confluence, and then released from the stretched states, thereby inducing an overcrowded condition. After 16 h of releasing, epithelial monolayers were fixed with 4% PFA and analyzed by immunofluorescence. For stretching assay, before cell seeding, silicone membranes were coated with 5 μg ml^{-1} fibronectin at 37°C for 1 h. Then, 8.0 × 10^5 normal MDCK cells were plated onto a silicone membrane and grown to confluence. To stretch membranes with the STB-100 cell stretcher system device, the silicone membrane was fixed in the device, and the one side of the membrane clamped to a movable shaft was pulled out from 20 mm to 24 mm, resulting in stretch of 20%, and kept for 5 min. Epithelial monolayers were fixed with 4% PFA and analyzed by immunofluorescence after releasing silicone membranes from the stretcher system device.

Quantitative Real-Time PCR

MDCK cells were cultured at a density of 6.5 × 10^5 cells in a 12-well dish. After incubation for 24ch, total RNA was extracted from the isolated cells using Trizol (Thermo Fisher Scientific) and RNeasy Mini Kit (QIAGEN) and was reverse-transcribed using a QuantiTect Reverse Transcription Kit (QIAGEN). GeneAce SYBR qPCR Mix (NIPPON GENE) was used to perform qPCR using the StepOne system (Thermo Fisher Scientific). We used β-actin as a reference gene to normalize data. COL17A1: 5′-ACTACTCAGAGCTGGCAAGC-3′ and 5′-CAGCCACAATGTCCTCCGTAG-3′; ABAT: 5′-AGCAAGAAGAAGCCCGCTGC-3′ and 5′-CTCAGACTGGATGGGCTCC-3′; ALDH5A1: 5′-GGCGTGGCTGCAGTCATCAC-3′ and 5′-GACAGTACAGCCGGCTGCCA-3′; GAD2: 5′-AAGCGGAGGTCAACTAT GCG-3′ and 5′-CATCACAGGCTGGCAGCAG-3′; β-actin: 5′-GGCACCCAGCACAATGAAG-3′ and 5′-ACAGTGAGGCCAGGATG-GAG-3′.

Mouse Pancreatic Cancer (KPC) Model and Immunohistochemistry

Animal protocols were approved by the Animal Care and Use Committee of Nagoya University Graduate School of Medicine. The KPC mouse model (LSL-KrasG12D/+; LSL-Trp53R172H/+; Pdx-1-Cre) was established as described previously[3]. Tissue sections prepared from early PanIN lesions at 8-10 weeks of age were subjected for immunohistochemistry. For immunohistochemistry on formalin-fixed, paraffin-embedded tissues, sections were deparaffinized with xylene and rehydrated with tap water, followed by immersion in an antigen retrieval buffer (Epitope Retrieval Solution pH 9.0, Leica) for 30 min at 98°C. The sections were washed three times in PBS and incubated in blocking buffer (X0909, Dako) for 30 min, followed by incubation with human anti-COL17A1 (20C5) (1:10,000) or rat anti-CD44 (1:100) antibody diluted with antibody diluent buffer (1% BSA, 0.1% NaN_3 in PBS) overnight at 4°C. The sections were washed three times with PBS and immersed in 0.5% H_2O_2 in methanol for 15 min for the inactivation of endogenous peroxidase. The sections were washed three times in PBS, followed by the incubation in EnVision+ System-HRP Labeled Polymer Anti-Mouse (Dako) for 30 min at room temperature. The sections were washed in PBS, incubated with Liquid DAB+ Substrate Chromogen System (Dako) for 5 min at room temperature, dehydrated in ethanol and cleared in xylene, followed by mounting with xylene-based mounting media Entellan new (Merck Millipore).

Metabolome Analysis

For metabolome analysis, 6.5 × 10^6 MDCK-pTR GFP-RasV12 or MDCK-pTRE3G GFP-RasV12 COL17A1-knockout 1-3 cells were first plated into a 10-cm dish. For each condition, cells were cultured in three dishes as triplicate. Upon plating, tetracycline was added to induce GFP-RasV12 expression. After incubation for 24 h, cells were washed twice with ice-cold 5% mannitol solution and covered with 1.0 mL of methanol containing 25 μM internal standards for 10 min. The resulting extracts were mixed with 200 μL of Milli-Q water and 400 μL of chloroform. The aqueous phase was then subjected to ultrafiltration. Metabolites of cells were quantified in each sample using CE-MS (Agilent Technologies, Santa Clara, CA) as previously described[55–58]. Briefly, to analyze cationic compounds, a fused silica capillary (50 μm i.d. x 100 cm) was used with 1 M formic acid as the electrolyte. Methanol/water (50% v/v) containing 0.01 μM hexakis(2,2-difluoroethoxy)phosphazene was delivered as the sheath liquid at 10 μL min^{-1}. ESI-TOFMS was performed in positive ion mode, and the capillary voltage was set to 4 kV. Automatic recalibration of each acquired spectrum was achieved using the masses of the reference standards ([13C isotopic ion of a protonated methanol dimer (2 MeOH+H)]+, m/z 66.0632) and ([hexakis(2,2-difluoroethoxy)phosphazene +H]+, m/z 622.0290). To identify metabolites, relative migration times of all peaks were calculated by normalization to the reference compound 3-aminopyrrolidine. The metabolites were identified by comparing their m/z values and relative migration times to the metabolite standards. Quantification was performed by comparing peak areas to calibration curves generated using internal standardization techniques with methionine sulfone. The other conditions were identical to those described previously[56]. To analyze anionic metabolites, a commercially available COSMO(+) (chemically coated with cationic polymer) capillary (50 μm i.d. x 105 cm) (Nacalai Tesque, Kyoto, Japan) was used with a 50 mM ammonium acetate solution, pH 8.5 as the electrolyte. Methanol/5 mM ammonium acetate (50% v/v) containing 0.01 μM hexakis(2,2-difluoroethoxy)phosphazene was

Please cite this article in press as: Kozawa et al., The CD44/COL17A1 pathway promotes the formation of multilayered, transformed epithelia, Current Biology (2021), https://doi.org/10.1016/j.cub.2021.04.078

delivered as the sheath liquid at 10 μL min^{-1}. ESI-TOFMS was performed in negative ion mode, and the capillary voltage was set to 3.5 kV. For anion analysis, trimesate and CSA were used as the reference and the internal standards, respectively. The other conditions were identical to those described previously[57]. CE-TOFMS raw data were analyzed using our proprietary software Master Hands (ver, 2.17.0.10). Briefly, the data processing for each experiment included data conversion, binning data into 0.02 m/z slices, baseline elimination, peak picking, integration, and elimination of redundant features to yield the all possible peaks lists. Data matrices were generated by an alignment process based on corrected migration times, and metabolite names were assigned to the aligned peaks by matching m/z and the corrected migration times of our standards library. Relative peak areas were calculated based on the ratio of peak area divided by those of internal standards, and metabolite concentrations were calculated based on the relative peak area between the sample and standard mixture.

Quantification of Glutathione

For quantification of glutathione, cells were incubated and treated under the same condition as metabolome analysis except that metabolites were extracted with 80% methanol. After removing the insoluble fractions by centrifugation, the supernatants were collected and dried using a SpeedVac at 30-45°C. Sample preparation was performed based on a previous study[59]. Briefly, TCEP solution was added to cell samples and incubated for 30 min at room temperature. After centrifugation, the supernatant was derivatized with ammonium 7-fluoro-2,1,3-benzoxadiazole-4-sulfonate (SBD-F) for 60 min at 60°C. For Bio-thiols separation, Inertsil ODS-4V (3.0 × 250 mm, GL Sciences, Tokyo, Japan) was used as the stationary phase. Mobile phase was 100 mM acetate buffer, pH 4.0/MeOH (97.5/2.5, v/v) at a flow rate of 0.4 mL min^{-1}. The SBD-thiols were detected by fluorescence with excitation and emission wavelengths of 375 and 510 nm, respectively.

QUANTIFICATION AND STATISTICAL ANALYSIS

For data analyses, paired two-tailed Student's t tests, unpaired two-tailed Student's t tests, Mann-Whitney test, or one-way ANOVA with Tukey's test were used to determine P values. P values less than 0.05 were considered to be significant. No statistical method was used to predetermine sample size.